

Charles University in Prague
Faculty of Mathematics and Physics

MASTER'S THESIS



Ladislav Fekete

Materials for Solar Cells Based on Thin Silicon Films

Institute of Physics of Charles University
Supervisor: Doc. RNDr. Vladimír Baumruk, CSc.
Study programme: Physics
Specialization: Optics and Optoelectronics

Acknowledgements

The major deal of this work was done in the Department of Thin Films, Institute of Physics, Academy of Sciences of the Czech Republic and in the Institute of Physics of Charles University in Prague and the Raman spectra measurement were performed in the MicroRaman laboratory, the Academy of Sciences of the Czech Republic.

First of all I would like to thank Doc. V. Baumruk, my supervisor, for his guidance and support which has contributed immensely to the successful completion of my studies.

I am grateful to Dr. A. Fejfar for his guidance, patience, understanding and teaching experience which gives me the knowledge of the programming in Delphi and many different other experimental experiences.

I want to express many thanks to K. Kůsová for helping with writing in L^AT_EX, ing. I. Drbohlav for measuring the samples by the AFM and ing. I. Gregora for technical support at measuring the Raman spectra.

For the preparation of the samples I would like to thank ing. J. Stuchlík from the Department of Thin Films and Dr. Manabu Ito from Toppan Printing company.

My special thanks belong to Dr. J. Kočka, head of the Department of Thin Films, and all laboratory staff for fruitful discussions, technical assistance and friendly atmosphere. Without trying to be complete, I would like to mention ing. T. Mates, Dr. P. Fojtík, Mgr. M. Ledinský, Dr. Ha Stuchlíková and Dr. K. Luterová.

Last but not least, I would like to thank my family and friends for all the support, patience, encouragement and friendship they provided.

I hereby state that I have written this master's thesis by myself using only the cited references. I agree to lend it.

Prague, 16 April 2004

Ladislav Fekete

Contents

Abstracts	3
1 Introduction	4
1.1 Solar Energy and Solar Cells	4
1.2 Structural and Electrical Properties of Silicon Films	6
2 Raman Spectroscopy	8
2.1 Light Scattering Mechanism and Selection Rules	8
2.2 The Raman Spectra of Microcrystalline Silicon	10
2.3 Methods of Obtaining Crystallinity from Raman Spectra	11
2.4 Motivation of This Work	14
3 Measuring the Raman Spectra	16
3.1 The Charles University Laboratory	16
3.2 The Academy of Sciences Laboratory	17
3.3 Measurements of the Raman Spectra	18
4 Marquardt-Levenberg Algorithm	22
4.1 Parameter Estimation by the Non-Linear Least-Square Fitting	22
4.2 Statement of the Problem	23
4.3 The Marquardt-Levenberg Method	25
5 Program DOORS	26
5.1 Operating the DOORS Program	26
5.2 Universal Function for the Amorphous Part of the Spectrum	33
6 Samples	34
6.1 Different Series of Samples	37
6.1.1 The 54 MHz Dilution Series at Temperature of 80°C	37
6.1.2 The Manabu Ito Temperature Series	39

6.1.3	The STM RF Temperature Series	41
7	Results	44
7.1	Amorphous Samples	44
7.2	Fitting the Amorphous Spectra	45
7.3	Fitting the Microcrystalline Spectra	47
7.4	Series of the Nucleation Density on the Sample Stm282	50
7.5	Nucleation Density on the Samples Stm254	56
7.6	Manabu Ito Dilution Series (MDS)	62
7.7	Manabu Ito Temperature Series (MTS)	66
7.8	RF STM Temperature Series (RFTS)	71
8	Discussion	76
8.1	Background	76
8.2	Amorphous Samples	76
8.3	Subtracting the Amorphous Part of the Microcrystalline Spec- trum	77
8.4	Complications of the Micro-Raman Measurements	78
8.5	Different Fitting Methods	78
8.6	Crystallinity Evaluation	80
8.7	Future Plans	81
9	Conclusion	82

Title: Materials for Solar Cells Based on Thin Silicon Films

Author: Ladislav Fekete

Institute: Institute of Physics of Charles University

Supervisor: Doc. RNDr. Vladimír Baumruk, CSc.

Supervisor's e-mail address: baumruk@karlov.mff.cuni.cz

Abstract: Thin film microcrystalline silicon is the most promising material for large area PN junction solar cells. As microcrystalline silicon is a heterogenous material composed of two phases (amorphous silicon tissue from which crystalline grains of micrometric dimension grow). The Raman spectra are commonly used to determine the crystallinity of mixed phase silicon thin films by analyzing the contributions of amorphous and crystalline phase to TO phonon band. Many different empirical or semi-empirical methods of evaluating crystallinity from the Raman spectra exist. In this master's thesis the microcrystalline Raman spectra were studied and a better way of evaluating crystallinity was searched for. The decomposition of the microcrystalline spectra of the series of the samples, where a single deposition parameter was changing, by fitting them with Gaussian bands was performed. We also report on the development of a special software for the band decomposition by non-linear least-squares fitting based on Marquardt-Levenberg algorithm and demonstrate its use for a series of films with structure changing from amorphous to fully microcrystalline.

Keywords: Raman scattering, crystallinity, $\mu\text{c-Si:H}$ and a-Si:H

Chapter 1

Introduction

1.1 Solar Energy and Solar Cells

Sun, our nearest star, produces in its core an enormous amount of energy. This energy comes from a fusion reaction, where a helium atom is created from hydrogen atoms. Sun's power is about 3.85×10^{23} kW. This energy is radiated in all directions. On the illuminated part of the Earth only a fraction of this power incidents, which is about 175,000 TW. That is approximately 1.3 kWm^{-2} at the outer edge of atmosphere. Because of losses in the atmosphere caused by absorption and scattering the power flux density on the surface of the Earth is approximately 1 kWm^{-2} with spectral distribution AM1.5 (atmospheric mass 1.5) shown in the figure 1.1 .

Solar cells use photovoltaic effect, observed first in 1839 by Edmond Becquerel, converting solar energy to electric energy. The most common solar cells are large area semiconductor PN junctions, where the incident photons with energy greater than the energy of the band gap create electron - hole pairs. Because of the PN junction voltage the electron and the hole are separated and the photocurrent and photovoltage appear. In the figure 1.2 current-voltage dependance of the PN junction without and under illumination is shown.

If the PN junction is illuminated, the current-voltage dependence shifts and the device can produce energy. Output power P is computed as

$$P = IU. \quad (1.1)$$

The simplest variable which gives us the information about solar cell performance is the efficiency η defined as the ratio of the maximum output power P_{max} to the power of the incident light P_{in} :

$$\eta = \frac{P_{max}}{P_{in}} \quad (1.2)$$

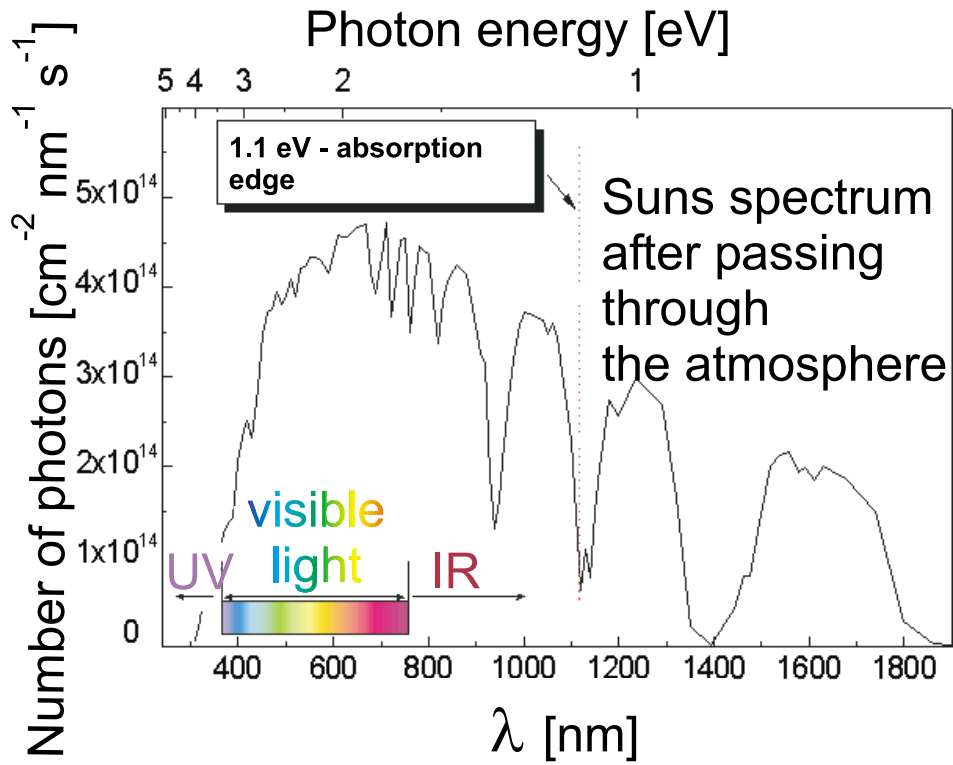


Figure 1.1: Sun spectrum after passing through the atmosphere. The monocrystalline silicon solar cell absorbs photons with energy greater than 1.1 eV [1]

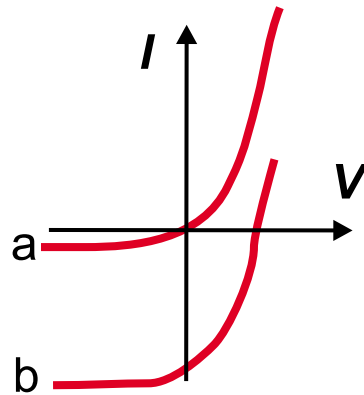


Figure 1.2: The current-voltage dependence on the PN junction without (a) and under (b) illumination.

A silicon material with the highest efficiency is the mono- or polycrystalline silicon. The highest monocrystalline silicon solar cell efficiency is 24.7 % [2], which is very close to the theoretically achievable efficiency of around 27 % [3]. Routinely sold solar cells have efficiencies around 16 %. Their wider use is hindered by high price, due mainly to the cost of silicon wafers. Production of the crystalline silicon requires a lot of energy, so that the energy payback time is around 5 years. Thin film solar cells are studied as a way how to reduce the energy required for the solar cell production and eventually also the cost.

1.2 Structural and Electrical Properties of Silicon Films

The most promising material for thin film solar cells seems to be silicon because of its huge resources and well-known preparing technology.

Amorphous silicon (a-Si:H) is one of the most used materials for thin film solar cells. Its silicon bonding structure is similar to crystalline silicon, but only for a few silicon atom neighbours. At greater distances the lattice periodicity is disturbed by disorder. The disorder relaxes \vec{k} selection rules and causes greater absorption than in crystalline silicon. The dangling bonds are also the result of disorder. They appear when the stress of the silicon covalent bonds is too high and some bonds break. The dangling bond defects act as efficient carrier recombination centres. Their total density is not constant: it can be decreased by annealing, or on the other hand increased by illumination. This is the reason why the efficiency of amorphous solar cells decreases. The majority of dangling bonds can be passivated by adding hydrogen during deposition

Microcrystalline silicon (μc -Si:H) is a thin film material which consists of small crystalline grains with sizes between 5 nm and 300 nm embedded in an amorphous tissue (figure 1.3). The μc -Si:H layer growth starts with amorphous layer in which the crystalline nuclei grains arise. Their density can be controlled by the substrate or deposition parameters. With continuing growth the grains connect and interconnected microcrystalline layer is formed. While the presence of the isolated grain aggregates improves the photoconductive properties before the percolation threshold is reached, further increase in crystallinity may have opposite effect due to detrimental role of increasing concentration

of the defective grain boundaries [4]. The columnar growth of the crystals leads to a naturally rough surface which results in an enhanced light scattering effect [4].

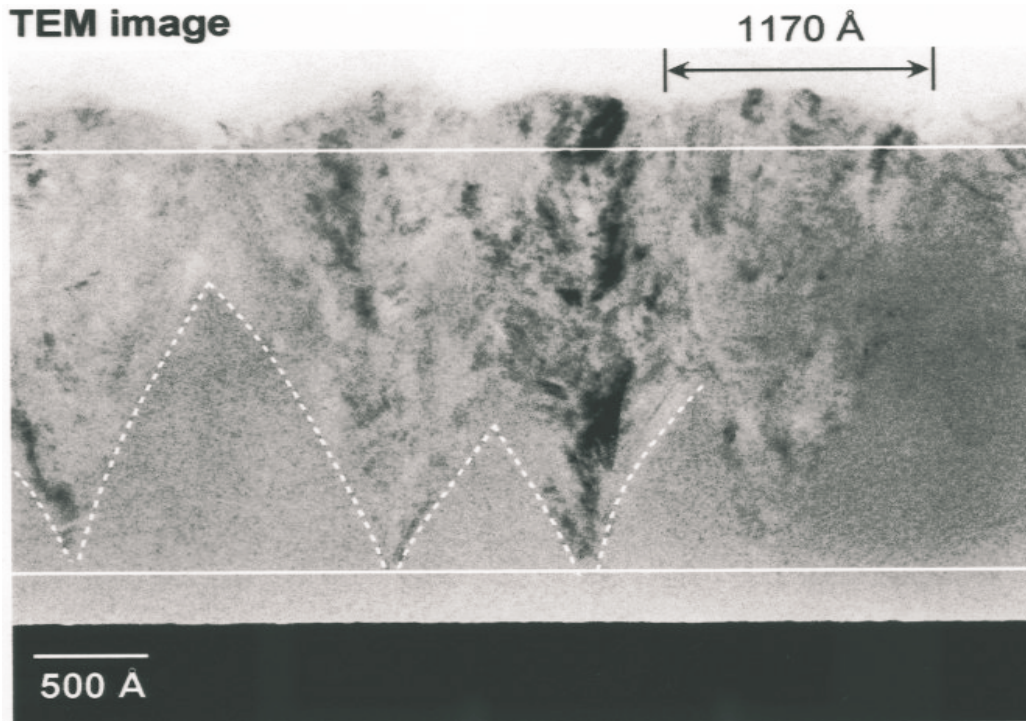


Figure 1.3: TEM image [5] illustrating the microcrystalline silicon growth stages: the amorphous incubation layer, the grain nucleation and growth and the creation of the grain boundaries. The grains are also responsible for the natural surface roughness.

The microcrystalline silicon is a material with a wide of application potential not only in solar cell industry, but in the whole thin film production. Now it is possible to buy not only mobile phones but also computer displays or TV screens with amorphous silicon thin film transistors.

As many deposition parameters influence the structural and electrical properties of the microcrystalline thin films, the samples with different crystalline volume fraction (crystallinity) can be prepared. The crystalline volume fraction (i.e., ratio of the volume occupied by the crystalline phase to the total volume of the sample) can be obtained from the Raman spectroscopy.

Chapter 2

Raman Spectroscopy

Raman scattering was discovered by Raman and Krishnan in the 1920s. When a beam of monochromatic light is incident on a sample, some of the light is transmitted, some absorbed and some scattered. Most of the scattered light is scattered elastically with no change in frequency. This is called Rayleigh scattering. A tiny portion of the scattered light is shifted in frequency by the molecular vibrations and rotations or by the phonons in the sample. This type of scattering is called Raman scattering and the resulting spectrum is called a Raman spectrum. Raman spectra usually contain sharp peaks that are characteristic of phonons in the samples (in case of solid state samples) or of the vibrational transitions (in case of scattering on molecular species).

Although the inelastic scattered light was observed in 1920s, its weak intensity caused the real breakthrough of Raman spectroscopy to begin with the invention of lasers. Now, this kind of measurement can be built - "home made" in a laboratory with appropriate equipment, or can be bought as a complete commercial system.

2.1 Light Scattering Mechanism and Selection Rules

Raman spectroscopy belongs to the standard characterization methods of the microcrystalline silicon samples. Monochromatic scattered photons have energy increased or decreased by the energy of the phonon, which is caused by the deexcitation of molecules excited by incident light. Because of small differential cross-section (10^{-26} – 10^{-29} cm²/Sr) [6] the light source has to be intensive enough. Inelastic scattering processes are two-photon events that involve the simultaneous annihilation of an incident photon and the creation

of a scattered photon. The difference in the energy of the scattered $h\omega_S$ photon and the incident photon $h\omega_L$ is used for the creation or annihilation of the phonon. The event is called the Stokes process when the $h\omega_L > h\omega_S$ and the energy $h(\omega_L - \omega_S) = h\Omega$ is added to scattered medium and the phonon is created. If $h\omega_L < h\omega_S$ an elementary excitation of the scattered medium (phonon) is annihilated and the event is referred to as the anti-Stokes process. The intensity of the anti-Stokes process is strongly dependent on temperature, since this process can occur only when the medium is in excited state. The dominant form of the Raman scattering is the first order scattering, where a single quantum of excitation is involved. However, the creation or the annihilation of two or more quanta leading to a higher-order processes can be observed.

The interaction between a photon and a phonon is provided by an electron, which is excited to a virtual state, whose lifetime is approximately $10^{-13} - 10^{-14}$ s. In the first-order processes only the single elementary excitation participates. In such situations, momentum and energy conservation are required,

$$\vec{k}_L = \vec{k}_S \pm \vec{K} \quad (2.1)$$

$$h\omega_L = h\omega_S \pm h\Omega \quad (2.2)$$

where $h\Omega$ is the energy, \vec{K} is the momentum of the phonon and \vec{k}_L, \vec{k}_S are momenta of the incident and scattered photons, respectively.

The Raman effect can be explained as the interaction of the electromagnetic field of the incident radiation with a solid. The electric field may induce an electric dipole dependent on the deformation caused by the phonon mode. If the deformations caused by phonon mode are small, the polarizability can be expanded in the following series in the dependence of phonons amplitude u

$$\alpha = \alpha_0 + \alpha_1 u + \alpha_2 u^2 \dots \quad (2.3)$$

If the electric field of the incident radiation is $E(t) = E_0 \cos(\omega t)$ and the phonon amplitude is $u(t) = u_0 \cos(\Omega t)$, the dipole moment has a component:

$$\alpha_1 E_0 u_0 \cos(\omega t) \cos(\Omega t) = \frac{1}{2} E_0 u_0 [\cos(\omega + \Omega)t + \cos(\omega - \Omega)t] \quad (2.4)$$

Even though this model is simple it can explain the resulting frequency of the anti-Stokes photon as $(\omega + \Omega)$, where the phonon with frequency Ω

is annihilated and the frequency of the Stokes photon ($\omega - \Omega$), where the phonon with frequency Ω is created. The ratio of the intensity of the Raman anti-Stokes to Stokes lines is predicted to be [7]

$$\frac{I_{AS}}{I_S} = \left[\frac{\omega + \Omega}{\omega - \Omega} \right]^4 e^{-\frac{\hbar\Omega}{kT}} \quad (2.5)$$

The Boltzmann exponential factor is the dominant term in the equation, which makes the anti-Stokes features of the spectra much weaker than the corresponding Stokes lines, which is why Raman scattering is mostly measured in the Stokes part of spectra.

2.2 The Raman Spectra of Microcrystalline Silicon

In the crystalline material only the phonons with zero momentum are selected because of the momentum conservation law. In the monocrystalline silicon only the TO phonons with $K \simeq 0$ with the energy of 64 meV have zero momentum, which leads to a sharp peak at the Raman spectra centred at 520 cm^{-1} . In the amorphous silicon the momentum selection rule is relaxed and the Raman scattering occurs with phonons from the whole Brillouin zone. The first order Raman spectra of amorphous silicon thus reflect the weighted phonon density of states (DOS) and are distributed between 0 and 500 cm^{-1} . The spectra show four distinct bands corresponding to different network vibration modes. The sharp TO peak at 520 cm^{-1} of c-Si corresponding to the upper $k = 0$ point of TO phonon DOS is replaced by a broader band centred at around 480 cm^{-1} resulting from the whole TO band of the phonon DOS. This band dominates the Raman spectra of amorphous silicon, but often three other bands can be distinguished, corresponding to: the LO phonon, centred at 380 cm^{-1} , the LA-phonon, centred at 310 cm^{-1} and the TA-phonon, centred at 150 cm^{-1} [8].

The position and the width of the a-Si:H TO band is often used as a measure of the bonding disorder [9]. It was observed that the TO band in a-Si:H Raman spectra depends on the hydrogen content [10], alloying with elements such as carbon or nitrogen [11], residual stress in the a-Si:H films [12], all of which influence the Si-Si bonding disorder. These factors affect not only the shape of the TO band, but also of other bands, resulting in changes of their relative intensities.

The microcrystalline Raman spectrum unfortunately is not the sum of pure amorphous and pure single crystalline spectra. As the spectra of the

small crystallites differ from the spectra of crystalline silicon the size of the microcrystallites has influence on the microcrystalline Raman spectra.

2.3 Methods of Obtaining Crystallinity from Raman Spectra

The crystalline volume fraction is a crucial parameter with the influence on the mobility and lifetime of the photogenerated charge carriers deciding the applicability of the microcrystalline material for the solar cells. As the Raman spectra of the microcrystalline silicon are complex, a variety of methods for obtaining crystallinity exists. For computing the crystallinity it is necessary to determine which part of the spectra is attributed to the amorphous phase and which to the crystalline phase.

The DOS of the amorphous silicon is quite similar to that of the crystalline silicon, aside from a broadening of about 25 cm^{-1} [9]. The comparison of the DOS for a-Si:H as measured from neutron and Raman scattering and the theoretical calculations of the c-Si are shown in the figure 2.1.

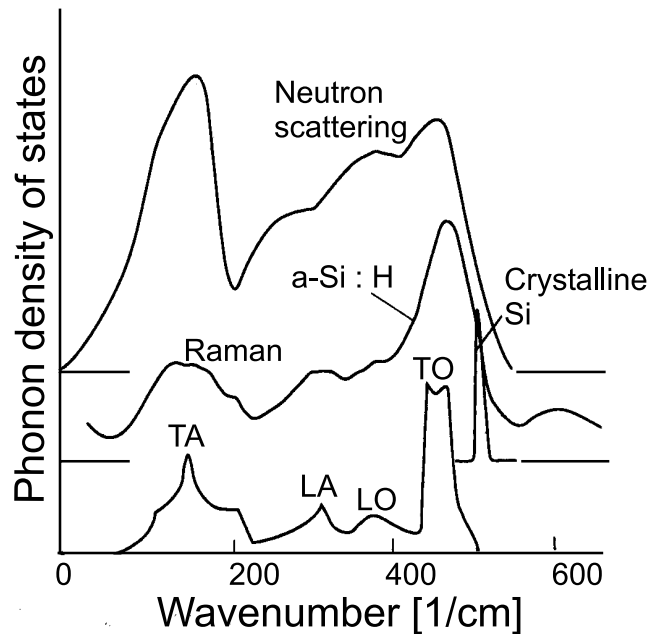


Figure 2.1: *a-Si:H* phonon density of states as derived from neutron scattering compared with Raman spectra of *a-Si:H* and theoretically calculated *c-Si* phonon density of states [9].

The theoretical approach with the goal to correlate the vibrational struc-

ture with the modelling of the continuous random network has had only a limited success [13]. The strongest vibrational signals from the TA and TO amorphous silicon phonons, can be well reproduced by the simplest models which require only tetrahedral coordination and the existence of non-central force. However, the details of the spectrum can be obtained only with the full continuous random network model. The structural models can be divided into three categories: finite (200-500 atoms) hand-built models, computer-generated periodic distorted network models with 60 to 500 atoms in a unit cell and finally the Bethe lattices. The best approximations of the amorphous materials can be obtained from the computer-generated models using the computing power of supercomputers. The models can be prepared either by quenching fluid in a molecular dynamics or by distorting an initially crystalline lattice by bond-breaking and relaxation. The study of such a complicated problem for all our amorphous or microcrystalline samples is not possible.

Physical interpretation of the Raman spectra of disordered silicon should start with a model of phonon DOS and inelastic scattering cross-sections, but this approach is too complicated for a common everyday evaluation of the structure of silicon thin films.

The presence of four distinct bands in a-Si:H Raman spectra (see figure 2.1) led to efforts to decompose the Raman spectra into several peaks. Various spectral shapes were tested, including Gaussian bands, Lorentzian or skewed Lorentzian bands [12], Fano shape [14], etc. This approach is empiric, yet it is the only practical way for example for evaluating crystallinity of the mixed phase microcrystalline films.

The microcrystalline silicon is a heterogenous material composed of amorphous and crystalline silicon material. Due to this fact signals from both phases are present in the Stokes Raman spectra.

The Raman spectra of the fully microcrystalline silicon thin film is dominated by the TO phonon band with positions at around 510 to 515 cm^{-1} . The small crystallite size is responsible for the shift of the band to lower wavenumber from the c-Si value of 520 cm^{-1} and for its widening to $<$ or $\sim 10 \text{ cm}^{-1}$. The TO phonon band shape in microcrystalline silicon is clearly distinct from a-Si:H. This forms the basis for the evaluation of crystallinity of the mixed phase silicon films from Raman spectra.

The crystallinity as a ratio of I_{MAX} and I_{480} The simplest method to obtain the crystallinity is to compute the crystallinity using the ratio of the maximum of the Raman spectrum crystalline amplitude I_{MAX} and Raman spectrum amplitude I_{480} at 480 cm^{-1} as in equation below (see figure 2.2).

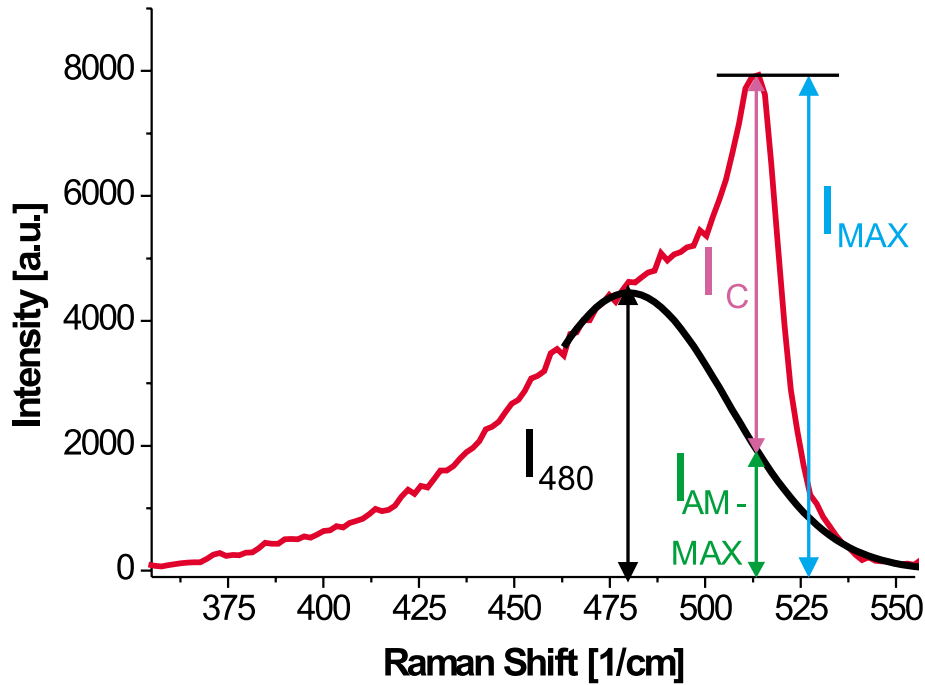


Figure 2.2: The crystallinity evaluation from the amplitudes of the Raman spectra. I_{480} is amplitude at 480 cm^{-1} , I_{MAX} is the amplitude of the maximum Raman signal and the I_C is the I_{MAX} amplitude reduced by the contribution of the amorphous signal at the wavenumber of the maximal Raman signal I_{AM-MAX} .

$$X_C = \frac{I_{MAX}}{I_{MAX} + 1.25I_{480}} \quad (2.6)$$

The number 1.25 is an empirical constant whose physical meaning is ascribed to different Raman scattering cross sections of amorphous and microcrystalline structures and whose value was found by comparison with independent crystallinity determination methods, such as XRD [15]. This method gives only very rough estimate of the crystallinity of the material. However, for highly crystalline samples this method is sufficient.

The corrected ratio method where the shape of the broad amorphous signal is taken into account. As the result I_C , instead of I_{MAX} , is taken as a crystalline contribution [16] (see figure 2.2). The crystallinity is

computed as in equation

$$X_C = \frac{I_C}{I_C + 1.25I_{480}} \quad (2.7)$$

The crystallinity as a ratio of the peak areas The microcrystalline spectra are often decomposed to the amorphous and the crystalline part by fitting two curves [17]. For example the Gaussian and the Lorentzian or two Gaussians line profiles can be used for the description of spectra. Unfortunately, this procedure does not lead to a good fit and broad amorphous peak tends to shift from 480 cm^{-1} to higher energies than expected.

$$X_C = \frac{S_C}{S_C + yS_A} \quad (2.8)$$

The S_A is the area of the amorphous TO phonon, the S_C is the area of the crystalline TO phonon, and finally, y in the equation corresponds to the ratio of cross-sections of the crystalline phonon excitation compared to amorphous. It is usually set to 0.8 but it varies from 0.7 to 0.9 as the crystallite size ranges from 15 to 5 nm [18], [19].

Crystallinity from three-peak peak fitting In order to obtain a better fit the Raman spectrum is often decomposed to three Gaussian peaks [20] [21] [22]. The third peak is attributed to the grain boundaries. The crystallinity can be computed from the equation below:

$$X_C = \frac{S_C + S_{GB}}{S_C + S_{GB} + yS_A} \quad (2.9)$$

The last approach (fit by three Gaussians) requires nine fitting parameters and even then quite often the fit is not very good. Using more complicated spectral shapes or increasing the number of peaks for improving the fit leads to a danger of parameter correlation and large uncertainty in the estimated values. This problem is made even worse by possible systematic errors introduced by the background subtraction.

2.4 Motivation of This Work

The above mentioned methods are the most frequently used ways to compute the crystallinity of mixed phase silicon layers. Unfortunately, there is not a uniform procedure and many laboratories use their own approach to this

problem which implies that different values of such an important parameter as the crystallinity can be evaluated from the same sample spectrum by different working groups.

In other words: Raman spectra of amorphous, nano- and micro-crystalline silicon are well understood and a large amount of published results is available in this field. However, no standard simple procedure for evaluating crystallinity and other parameters seems to exist. Our goal was to search for such a procedure.

The importance of this goal is evident from the following: The research in our laboratory in the Department of Thin Films, Institute of Physics, AS CR is oriented to the study of thin microcrystalline silicon films for photovoltaic and other applications. Up to 100 samples of mixed phase silicon thin films are deposited yearly and Raman spectra (often in several locations) are measured as a part of their characterization. The motivation for this thesis was a critical reexamination of the Raman spectra evaluation in the whole database of the available spectra.

Many sample depositions are arranged in series in which we studied an influence of a single technological parameter, for example substrate temperature, dilution of silane in hydrogen or the thickness of the films. The most interesting are the series in which the parameter change led to a transition from amorphous to fully microcrystalline growth.

This opens a possibility to follow the influence of the deposition parameter on the whole series of Raman spectra. In addition, the spectra can be correlated with a large amount of other experimental results, including direct observation of the films structure by atomic force microscopy.

Therefore, the goals of this work were as follows:

- 1) to fit the whole series of Raman spectra with changing crystallinity by different fitting functions
- 2) to look for the correlations between the fit parameters and the quality of the fit with other experimental results
- 3) finally, to provide a simple standard way for evaluating the crystallinity.

The principal task of the diploma thesis was to develop a dedicated program for non-linear least squares fitting of the Raman spectra series. The necessity for this resulted from the previous diploma thesis [16] which opened this topic. The comparison of the noise and quality of the background of different Raman spectra led to the necessity of remeasurement of several spectra, this time using a micro-Raman spectrograph with a better signal to noise ratio. Finally, we have used special samples with crystallinity changing with position on the substrate were also studied and this required a study of their surface by atomic force microscopy.

Chapter 3

Measuring the Raman Spectra

Our measurements were performed in two different laboratories, the first of which is the Raman spectroscopy laboratory of the Charles University and the second one is the Raman spectroscopy laboratory of the Academy of Sciences. In the following text these two different spectrographs be will presented.

3.1 The Charles University Laboratory

The experimental setup is shown in the figure 3.1.

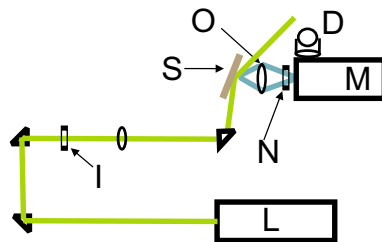


Figure 3.1: The scheme of the experimental setup of the Charles University laboratory of Raman spectroscopy. The excitation light is generated in the continuous-wave (CW) argon ion laser (L) and focused on the sample (S). The laser plasma radiation is filtered by the interference filter (I). The inelastic scattered light is focused with the objective (O) on the entrance slit of the spectrograph (M). The Rayleigh elastic scattering is filtered by the notch filter (N). The spectrum is measured by the CCD detector (D)

The source of the excitation light is a continuous-wave argon ion laser *Coherent Innova 305* at the wavelength of 514.5 nm. Before the light is focused to the sample, the argon plasma radiation is filtered by a interference

filter. After the laser beam is introduced to the sample, the non-elastic scattered light is focused by an objective lens (*Pancolar 1,8/80 Carl Zeiss Jena*) to the slit of the spectrograph in 90 degrees reflective configuration. The intensity of Rayleigh elastic scattering is reduced by a "notch" filter (*Kaiser optical system*) with the optical density greater than 6. Regarding the spectrograph (*Monospek 600, Hilger and Watts, f/5.6*), at the Czerny-Turner configuration is used. The dispersive element is a holographic grating (*100 mm × 100 mm with groove density 1200 gr/mm from Milton Roy*) and the entrance slit is adjustable with a micrometric screw in the range of 0 – 12 mm with an accuracy of 5 μm . Next to the spectrograph is the CCD detector (*LN Princeton Instruments*) is located. The studied part of the spectrum is chosen by the rotating grating. The CCD detector is composed of 1024×256 pixels, each of them square shaped with a side of 27 μm , which together form a rectangle with an area of $6,9 \times 27,6 \text{ mm}^2$. As the detector's dark signal is low, it is cooled by liquid nitrogen to $-120 \text{ }^\circ\text{C}$.

3.2 The Academy of Sciences Laboratory

The scheme of the experimental setup of the Academy of Sciences MicroRaman laboratory is shown in the figure 3.2.

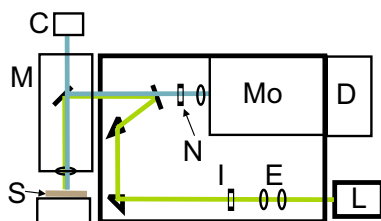


Figure 3.2: The scheme of the experimental setup of the Academy of Sciences MicroRaman laboratory. The excitation light is generated in the CW argon ion laser (L). The laser beam is expanded in the expander (E) and then focused on the sample (S) in the microscope (M). The laser plasma radiation is filtered by the interference filter (I). The inelastic scattered light is guided on the slit of the spectrograph (Mo). The Rayleigh elastic scattering is filtered by the notch filter (N). The spectrum is measured by the CCD detector (D). The microscope is equipped with the CCD camera (C) for recording the images of the sample surface.

The Micro Raman spectroscopy laboratory is equipped with a commercial instrument *Renishaw RM 1000* composed of an optical microscope *Leica* allowing the optical magnification of 50, 200, 500, 1000 times, a CW argon

ion laser at the wavelength of 514.5 nm, a CCD detector with a low dark signal and low readout noise, which is thermo-electrically cooled to $-70\text{ }^{\circ}\text{C}$, and finally the confocal micro-spectroscope with the spectral resolution of 1 cm^{-1} , the spatial resolution of $2\text{ }\mu\text{m}$ and the holographic grating with groove density 1800 gr/mm and optical efficiency greater than 30 %. In order to take images from the measured part of the sample, a CCD camera is connected to the microscope.

3.3 Measurements of the Raman Spectra

The microcrystalline silicon material has been studied in the Department of the Thin Films in Academy of Sciences for several years because of the possible applications in solar cells. As the Raman spectroscopy measurements belong to standard characterization techniques, a large database of Raman spectra exists. The majority of these measurements was performed in the Raman spectroscopy laboratory at Charles University. Unfortunately, this database contains mainly spectra which are not of a sufficient quality for the comparison of fitting by different functions and for searching for the details. There are two main reasons for this:

a) the signal-to-noise ratio of the spectra was too low. This problem was overcome by measuring or remeasuring spectra in the MicroRaman laboratory at the Academy of Sciences. This is demonstrated in the figure 3.3, which shows the spectrum measured in 2001 in the Raman laboratory at the Charles University compared to the spectrum of the same sample measured by the MicroRaman setup at the Institute of Physics.

b) the problem with the spectra background.

The spectra were of sufficient quality for obtaining the crystallinity by simple procedure (see figure 3.3) but were too noisy for fitting. We want to demonstrate in the figure 3.3 that the amorphous spectra are not detailed enough in our database.

Almost all of these spectra have polyline background subtracted, which can introduce a systematic error. The spectra measured from 2001 are available also as raw data, which means without the subtracted background.

The third problem was that the experimental setup was sensitive to adjusting, so the background could change by repeated mounting. To minimize the effect of the background, we have measured the Raman spectra more times for every sample (figure 3.4). Even then, only seldom was the background constant.

Different methods used in the past in our laboratory to subtract the background are shown in the figure 3.5 A, B, C. The subtraction of the

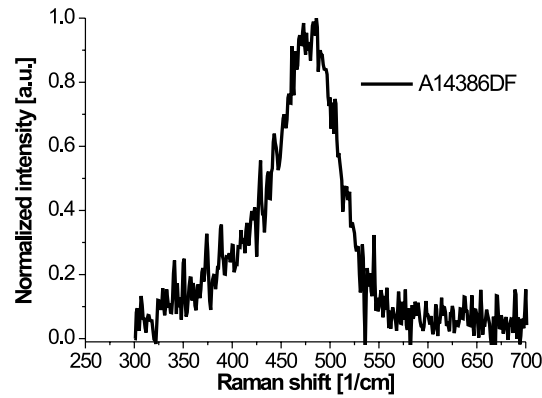


Figure 3.3: The spectrum, which was taken from the database of silicon spectra measured at the Charles University. As the spectrum had already the polyline background subtracted, it was not appropriate for fitting analysis.

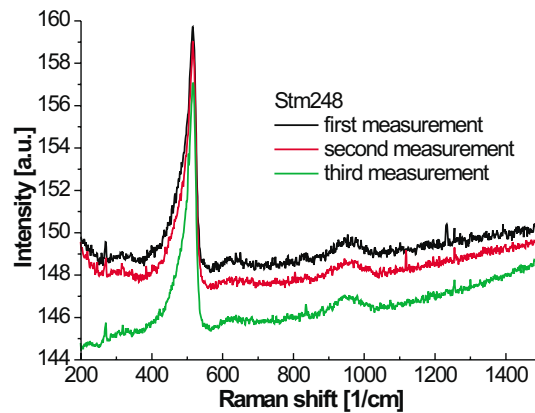


Figure 3.4: The changes of the background if we have measured the same sample three times one after another on the different locations of the sample.

polyline background was mostly used (A). The subtracting of the parabolic (B), or the parabolic with the Gaussian background (C) was used. The comparison of the subtraction of these methods is shown in the figure 3.5 D. The main idea of the subtraction was to extract the TO amorphous and TO crystalline signals. As the contribution of the LA and LO phonon is subtracted using this method which influence the remaining shape of the TO phonons, the introducing of an error is evident.

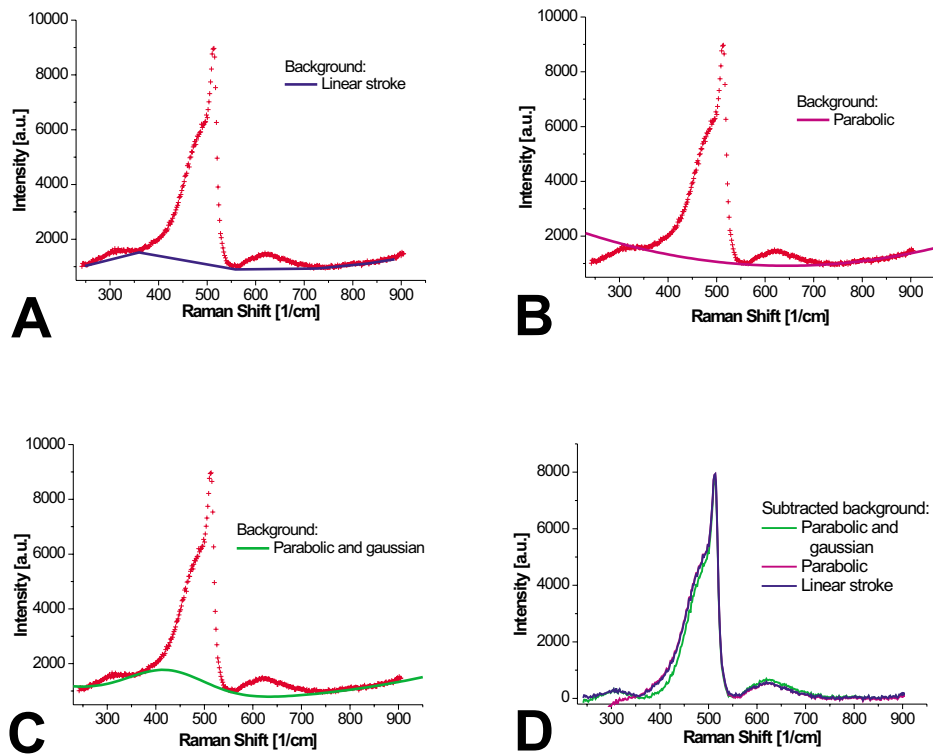


Figure 3.5: In the figure A, B and C the different methods to subtract the background are presented. The frequently used method is to subtract the poly-line background (A). If the background is not constant, the background as polynomial can be taken (B). The part of the spectrum, where the LA and LO phonon can be with a gaussian recompensed (C). In the last figure D are spectra without background shown.

The main advantage of MicroRaman spectroscopy laboratory in the Academy of Sciences for obtaining the detailed spectra is the fact that the measured spectra have much better signal to noise ratio and the background is almost constant even for amorphous samples (figure 3.6). By subtracting only the constant background the possible deformation of the spectra is minimized. In our further results only the spectra measured in MicroRaman laboratory will be discussed.

This experimental setup is also simpler to operate. The CCD camera connected to the microscope allows to get information in the concrete position of the excitation beam, so it is possible to choose a place on the sample which is without dust or other particles on the surface. It is often observed, if thin silicon films are under stress caused by the substrate or deposition

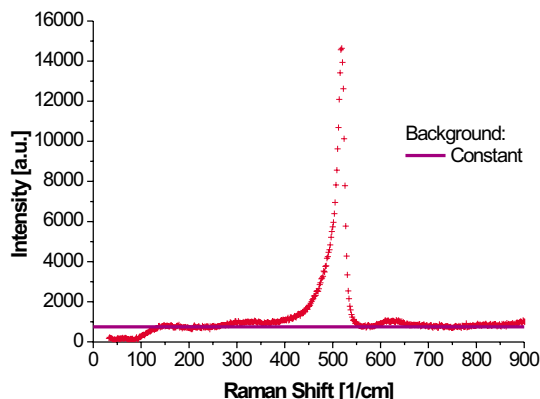


Figure 3.6: The constant background of the spectrum measured in the Micro-Raman laboratory in the Academy of Sciences. The edge of the notch filter is approximately at 150 cm^{-1}

conditions, that the films are unstable and can peel off. The optical view of the sample can help us to avoid measuring the peeled-off parts of the sample. The area of the spot of the laser beam can be modified by focusing or defocusing. The most focused spot has a diameter of about $2 \mu\text{m}$. At the full focus it is possible to crystallize the sample if the laser intensity is set to 100 percent (10 mW). To avoid the crystallization the laser beam was defocused to obtain the spot diameter of about $10 \mu\text{m}$ and the laser was set to 50 percent power or the laser intensity was reduced to 10 percent of the full power. The objective with 50 times magnification was used for all measurements. It was found empirically that 50 times 5 seconds accumulation time is optimal for the collection of spectra. Spectra were measured using the *Wire* program. The next advantage to the Charles University laboratory measurements was in spectra processing. It was not necessary to measure the spectrum of toluene for calibration before the sample spectrum [16] and the cosmic radiation creating the so called "spikes", was automatically removed. Additionally, simpler replacement of measured samples made the measurement much quicker so that approximately 60 spectra could be measured in one day in contrast to Charles University laboratory, where approximately 15 samples were measured in one day.

On the other hand, the main advantage of the Charles University laboratory is the dimension of the laser beam spot on the sample, which has approximately the radius of $15 \mu\text{m}$ as distinct from the MicroRaman laboratory, where the maximum laser beam spot diameter is approximately about $10 \mu\text{m}$.

Chapter 4

The Fitting of Raman Spectra with Program Based on Marquardt-Levenberg Algorithm

As the Raman spectrum is composed of signals from different phonons, the non-linear least-square curve-fitting is needed to extract the signal of the TO amorphous and the TO crystalline phonons, which are used for evaluating crystallinity. In this chapter Marquardt-Levenberg algorithm for non-linear least-square fitting will be presented.

4.1 Parameter Estimation by the Non-Linear Least-Square Fitting

Let the result of function Φ be a quantity (usually the sum of the squares of deviations of the fitting function and the data), which gives information about the "difference" between the fitting function and the experimental data. For all different combinations of n fitting parameters of the fitting function, the result of the function Φ creates a surface in n -dimensional space of the fitting parameters. If the fitting function is non-linear, the surface may consist of many hills and valleys. The task of the fitting algorithm is to find the lowest point in the lowest valley. In the lowest point there is the best approximation of the fitting function for the experimental data, because of the smallest difference between the fitting function and the experimental data. The minimization algorithm is able to find a way through the valley to the lowest point, but the starting point has to be in the proper (lowest)

valley. The best way to find the lowest point is to move from the starting point downhill as long as possible.

Finding the downhill direction is easy, it means just to calculate the gradient of the fitting function with respect to the adjustable parameters. The most complicated thing is to decide the size of the step. If the step is too big, it is possible to overstep the valley. In the proximity of the lowest point it is possible to expand the fitting function in Taylor series, thus linearize it and standard linear methods to get to the minimum in one step can be used. In greater distance from the lowest point the Taylor series is inaccurate, the guess of the step size is needed. If the guess is correct, Φ of the new set of parameters will decrease. Otherwise the step of smaller size is essential.

The Marquardt-Levenberg algorithm is actually the combination of these two methods. In the beginning of the process the gradient method is mainly used, but when the value of Φ gets smaller and smaller, the Taylor series method influences the fitting more and more. The gradient method converges rapidly far from the minimum but, in the contrast to the Taylor series method, near the minimum the convergence is slow.

4.2 Statement of the Problem

Let the $(x_1, y_1, \dots, x_n, y_n)$ be n data points, each with a standard deviation σ_n and a model fitting function $y = f(x; a)$; $a = a_1, a_2, \dots, a_m$ where x is the independent variable and a 's are adjustable parameters. The quantity Φ

$$\Phi = \sum_{i=1}^n \left(\frac{f(x_i; a) - y_i}{\sigma_i} \right)^2 \quad (4.1)$$

(frequently called χ^2 value for the fit) provides a measure of the fit by adjustable parameters, which has to be minimized so that the fitting function is optimal in least-square sense. If the fitting function f is linear in a 's, the shapes of constant Φ are ellipsoidal, and for optimization the standard methods can be used, setting

$$\frac{\partial \Phi}{\partial a_j} = 0 \quad (4.2)$$

for all j . If the fitting function f is not linear in a 's, the shapes of constant Φ are distorted and a number of valleys, each with its own local minimum, can exist.

Near the minimum Φ can be expanded in the Taylor series:

$$\Phi(x; a_0 + \delta a) = \Phi(x; a_0) + \sum_j \frac{\partial \Phi}{\partial a_j} \delta a_j + \sum_{j,k} \frac{\partial^2 \Phi}{\partial a_j \partial a_k} \delta a_j \delta a_k \quad (4.3)$$

For simplification it is suitable to define:

$$c \equiv \Phi(x; a_0) \quad b \equiv \nabla_a \Phi |_{x; a_0 + \delta a} \quad [H]_{j,k} = \left. \frac{\partial^2 \Phi}{\partial a_j \partial a_k} \right|_{x; a_0} \quad (4.4)$$

and then (4.3) can be written in the matrix notation

$$\Phi(x; a_0 + \delta a) = c - b \cdot \delta a + \frac{1}{2} \delta a \cdot H \cdot \delta a \quad (4.5)$$

where the matrix H , whose elements are the second partial derivatives of Φ with respect to the adjustable parameters, is called the Hessian matrix.

When the gradient of the previous equation is computed

$$\nabla_a \Phi |_{x; a_0 + \delta a} = H \cdot \delta a - b \quad (4.6)$$

the minimum (where the gradient vanishes) can be found by solving the equation

$$H \cdot \delta a = b \quad (4.7)$$

Upon a closer look the gradient of Φ has components:

$$b_j = \frac{\partial \Phi}{\partial a_j} \equiv -2 \sum_{i=1}^n \frac{[y_i - f(x_i; a)]}{\sigma_i^2} \frac{\partial f(x_i; a)}{\partial a_j} \quad (4.8)$$

and the Hessian matrix as a second partial derivative of Φ has components:

$$H_{j,k} \equiv \frac{\partial^2 \Phi}{\partial a_j \partial a_k} = 2 \sum_{i=1}^n \frac{1}{\sigma_i^2} \left[\frac{\partial f(x_i; a)}{\partial a_j} \frac{\partial f(x_i; a)}{\partial a_k} - [y_i - f(x_i; a)] \frac{\partial^2 f(x_i; a)}{\partial a_j \partial a_k} \right] \quad (4.9)$$

However the term multiplying the second partial derivative in this equation $[y_i - f(x_i; a)]$ is just the random error of each data point. When summing over i this term tends to cancel and can be ignored. Thus the simplification of previous equation is following:

$$H_{j,k} \equiv \frac{\partial^2 \Phi}{\partial a_j \partial a_k} = 2 \sum_{i=1}^n \frac{1}{\sigma_i^2} \left[\frac{\partial f(x_i; a)}{\partial a_j} \frac{\partial f(x_i; a)}{\partial a_k} \right] \quad (4.10)$$

Now, it is possible to step to the minimum of Φ by setting

$$a_{min} = a_0 + H^{-1} \cdot [-\nabla \Phi(x; a_0)] \quad (4.11)$$

This is called the Hessian method.

However, if the Taylor series approximation to Φ is not good enough, the step downhill direction can be recommended,

$$a_{new} = a_{initial} - constant \cdot [-\nabla \Phi(x; a_{initial})] \quad (4.12)$$

where the constant must be small enough so that the step is indeed downhill. This is called the gradient method.

4.3 The Marquardt-Levenberg Method

The Marquardt-Levenberg method [23] is a combination of gradient and Hessian methods. These two methods are bound together with the parameter λ , which presents weight which varies the importance from gradient method, far from the minimum, to Hessian method, as the minimum is approached.

Mathematically, the combination of the gradient and Hessian method is due to the definition of the new matrix

$$H'_{jj} = H_{jj}(1 + \lambda) \quad (4.13)$$

$$H'_{jk} = H_{jk} \quad (j \neq k) \quad (4.14)$$

and finding δa_j by solving

$$\sum_{j=0}^n H'_{jk} \delta a_j = b_k \quad (4.15)$$

When λ is very large, the diagonal terms in H' dominate, and the gradient method is used with a small step with the size of $1/\lambda$. As λ approaches zero, the Hessian method is used.

The following recipe for implementing the algorithm is recommended by Marquardt:

1. Choose a starting value a_O for parameters.
2. Compute $\Phi(a_O)$.
3. Pick a value for λ , say 10^{-3} .
4. If $\Phi(a_O + \delta a) > \Phi(a_O)$, increase λ by a factor of 10 and go back to step 4.
5. If $\Phi(a_O + \delta a) < \Phi(a_O)$, decrease λ by a factor of 10, replace a_O by $a_O + \delta a$ and go back to step 4.

Chapter 5

DOORS - Program for Decomposition of Ordinary Raman Spectra

The fitting program based on the Marquardt-Levenberg algorithm for fitting the Raman spectra of microcrystalline silicon has been developed. As the Raman spectra of the microcrystalline silicon are complicated and have not been sufficiently explained yet, the program may open the doors for us to better understand them. The program DOORS is designed to study a large quantity of spectra, fitting them with complicated functions and searching for which of them can describe the amorphous or crystalline parts of the spectrum in the best way.

5.1 Operating the DOORS Program

The program was made for fitting the Raman spectra, but it allows also a few pre-fitting operations with the spectra. The raw Raman spectra have background, which has to be subtracted. Mostly only a part of the spectrum is required to be fitted, so it is also possible to extract the interesting part of the spectrum. After fitting it is good to know if the fit was good enough. This information can be visually presented through residues.

Loading and saving the Data (*Load* and *Save* buttons)

After the program is executed, the *Load* button is enabled. The first step in the fitting program is to load the data for fitting. When the *Load* button is clicked, the user can search for a file with the data for fitting and open it.

After the data are loaded, other buttons become enabled (figure 5.1). One of them is the *Save* button, which allows the user to save data under different name to a selected path in the computer.

Printing or copying the graph (*Print* or *Copy picture* button)

The graphical output of the DOORS program is presented with copying the graph to the clipboard with the *Copy picture* button or printing the graph using the *Print* button (figure 5.1).

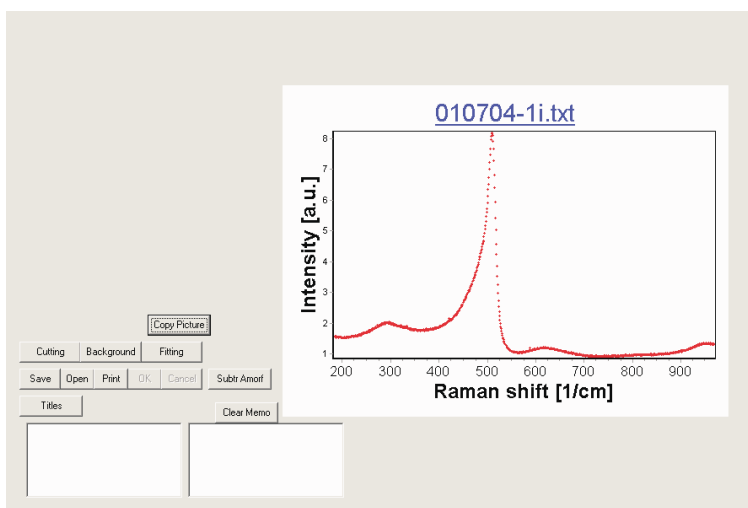


Figure 5.1: The main menu, where the buttons for cutting data, fitting, subtracting background or buttons for loading, saving and printing data can be chosen.

Changing titles (*Titles* button)

The graph title, titles of axes and their fonts can be changed in the form after the *Titles* button is clicked. The size of the axes labels can also be changed. By clicking the *OK* button, the modifications will be accepted (figure 5.2).

Figure 5.2: The form where the titles of the graph and axes can be changed.

Subtracting the background (*Background* button)

The parabolic, linear or Gaussian functions and their sum can be used for subtracting the background (figure 5.3).

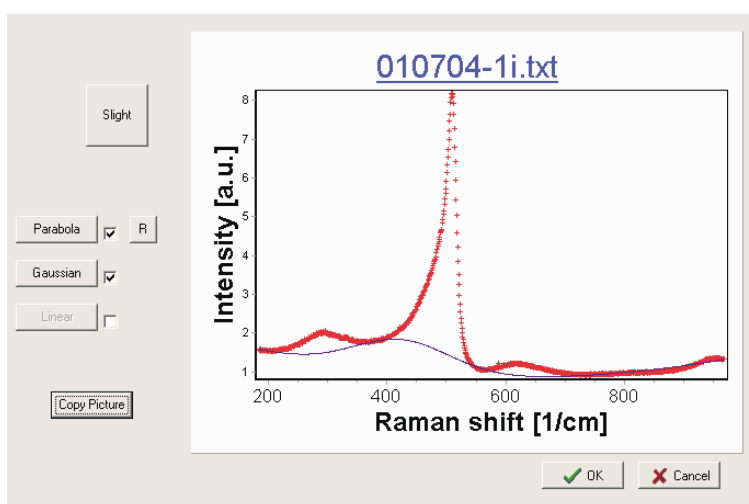


Figure 5.3: The form for subtracting the background.

Checkboxes next to the buttons with the names of the background functions signalize the presence of corresponding functions. If the unchecked checkbox is clicked, the corresponding function will be drawn into the graph. Using the Numpad keys it is possible to move the active function. The function starts to be active if the unchecked checkbox of corresponding function is clicked, or by clicking on an enabled button with the name of the function, which the user wants to be active. The sensitivity of the movement of the background function can be changed by clicking the square button with the name of the sensitivity of the step. The sensitivities are named *Very fine*,

Fine, *Slight*, *Middle* and *Rough* and the step sizes are corresponding to their names. If the active function is a parabola function, the shape of the curve can be flipped with *R* button. After adjusting the background functions, by moving them using arrows buttons on the numpad, the background with the the shape of the sum of all active background functions will be subtracted after clicking the *OK* button. The action can also be cancelled clicking the *Cancel* button. Finally, by pressing the *Copy picture* button, the graph is copied to the clipboard and can be pasted for example to a Microsoft Word document.

Choosing the part of the spectrum (*Cutting* button)

The *Cutting* button in the main menu serves for extracting the interesting part of the spectrum. After this button is clicked a new form appears. In the graph the spectrum and two vertical lines will be drawn. The part of the spectrum between these two lines will be chosen after the *OK* button is clicked. The line is active if it is green coloured (figure 5.4).

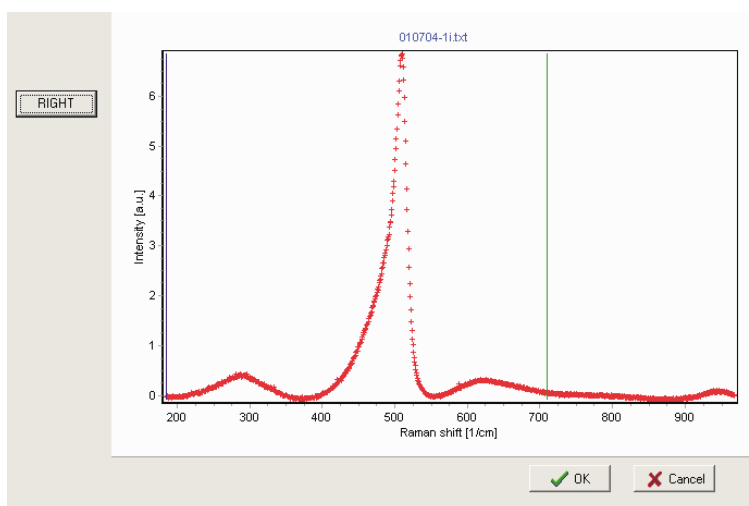


Figure 5.4: The form for selecting the interesting part of the data.

If its colour is blue, the line is inactive. Which of the lines is active can be decided with the button placed in upper part of the form. By clicking the button, the caption changes between *Left*, *Right* or *None* and the lines become active corresponding to the caption of this button. It is also possible to select the active line by clicking it. Moving the active lines is performed by *Left arrow* (4) or *Right arrow* (6) on the Numpad. The active line can also be moved to a new position by clicking the data point. With the *Cancel* or *OK* buttons the return to the main menu will follow.

Subtracting the amorphous part of the spectra manually (*Subtract Amorph* button)

Manual subtraction of the amorphous part of the spectrum can be done in the form after pressing the *Subtract Amorph* button. The file with the amorphous spectrum could be loaded by pressing the *Load Amorph spectra* button, where the path to the file has to be given correctly. When the amorphous spectrum is loaded, the amorphous spectrum is blue coloured and the difference between the amorphous spectrum and the spectrum for fitting (should be the fully microcrystalline part of the spectrum) is magenta coloured (figure 5.5).

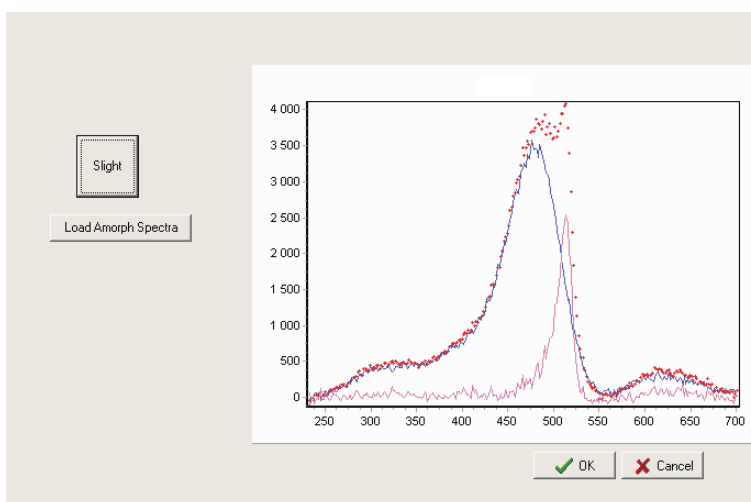


Figure 5.5: The form of subtracting the amorphous spectrum manually.

It is possible to move the amorphous spectrum pressing the *Up arrow* (8) or *Down arrow* (2). The movement is performed by multiplying the whole loaded amorphous spectrum by a constant number. The sensitivity of movement can be changed by pressing the square button named *Very fine*, *Fine*, *Slight*, *Middle* and *Rough* and the sensitivity of the movement corresponds to the caption of this button. If the amorphous spectrum is well adjusted, and the *OK* button is clicked, the subtracting of the amorphous spectrum will follow and only the crystalline part of the spectrum will remain.

Fitting the spectrum (*Fitting* button)

If the spectrum is without background, and the interesting part of the spectrum is chosen, the spectrum is prepared for fitting. By pressing the *Fitting* button, the Gaussian curve will be drawn in the graph. Its parameters are

written in the left part of the form into the labels. The parameters of the given fitting function always have the same colour as the drawn function. User can change the fitting function by clicking a corresponding combobox where the list of all possible fitting functions is provided. By pressing the *New* button a new fitting function is added. It is always a Gaussian, which can be changed by the user using the combobox. The sum of all presented fitting functions is black coloured. Next to all parameters there are checkboxes, which decide if the parameter will be taken as a fitting parameter, or if the parameter will be taken as a constant value. If there are more than two fitting functions, the last one can be deleted by the *Delete* button. For moving with the active fitting function, the following keys on the numpad are used: *Left arrow*(4), *Right arrow*(6), *Up arrow*(8), *Down arrow*(2), *Plus key*(+), *Minus key*(-), *Home key*(7), *PgDn key*(3), *PgUp key*(9), *End key*(1), and finally if the fitting function has 6 fitting parameters *Multiply key*(*) and *Divide key*(/). After adding a new function, the new function is always active. The active function can also be set by clicking the button of the number as the fitting function was added.

For fitting the series of the samples, where fitting with the same functions with approximately similar starting values of parameters is used, it is helpful to load this setup by pressing the *LoadIniFile* button. The setup is loaded from *AAAMultifittingFiles.ini* file. For all spectra of the series it is also possible to have an own set of the fitting functions with starting values of the fitting parameters saved in the *AAAMultifittingFiles.ini* file. Then the next set can be loaded with *NextIniFile* button. Above the fitting functions parameters the value of the least-square function Φ is written. If the user changes the parameters of the fitting functions by moving the fitting functions, or by entering the number in the edit of one of the parameters, the value of the function Φ will change according to the actual set of the parameters. After the rough setting of the fitting functions parameters, the fitting based on Marquardt-Levenberg algorithm can be initialized pressing the *Start* button. The algorithm will find the set of the parameters, where the value of the function Φ is minimal. When the fitting ends, the result of the fit can be seen in fitting function parameters, but more details, such as errors of the fitting parameters, will be written in the bottom part of the form into two memos by clicking to the *Add fit* button (figure 5.6).

Memos can be cleared pressing the *Clear Memo* button. In these two memos two different forms of numerical output are written. The second one is prepared as an output to *FittingOutput.dat* file, which is designed for the program ORIGIN. After clicking the *Copy text* button the first one is copied to the clipboard and can be pasted to for example the Microsoft Word document, and the second one is copied to the *FittingOutput.dat* file.

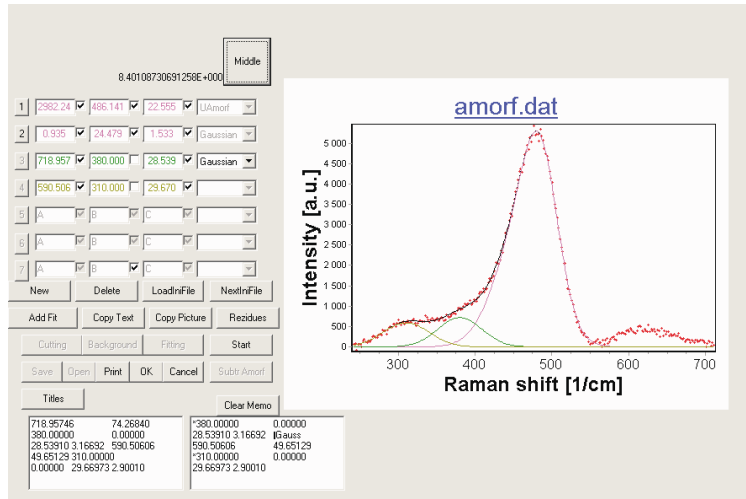


Figure 5.6: The form of spectrum fitting.

The third fitting output is in the same time copied to the *FittingOutput.ini* file. Here the functions and their parameters are written in the same way as they have to be written in the *AAAMultifitingFiles.ini* file, by which the set of fitting functions and their parameters can be loaded before fitting. So this is the way to prepare such a set, when the data are copied from the *FittingOutput.ini* to the *AAAMultifitingFiles.ini* file. The difference between the fitting function and the data set can be seen after the *Residues* button is clicked (figure 5.7).

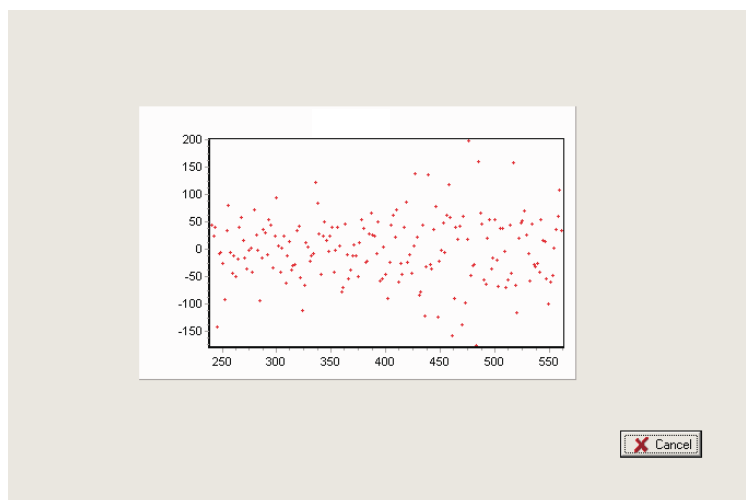


Figure 5.7: The difference between the data and the fit.

5.2 Universal Function for the Amorphous Part of the Spectrum

For the fitting of the amorphous TO phonon a universal function named UAmorph was suggested. As the signal from the amorphous TO phonon is not symmetrical and the shape of this signal can be described with two Gaussian peaks, the UAmorph function is a combination of two Gaussian curves. In fact, it is exactly the sum of the two Gaussian peaks. So what makes this function so special? It is its parameters. The first three parameters are the parameters of typical a Gaussian: the amplitude, the centre and the width. The spare three parameters are not the amplitude, the centre and the width of the second Gaussian, but the ratio between the amplitudes, the distance of the centres and finally the ratio between the widths of these two Gaussians.

Chapter 6

Samples

In the laboratory of the Academy of Sciences one of the most common deposition procedures Plasma Enhanced Chemical Vapour Deposition (PECVD) is used for preparing the microcrystalline thin silicon films (figure 6.1). In this procedure the silane or silane diluted in hydrogen is decomposed by a plasma discharge and the thin film grows on glass or PET substrates. In order to understand the influence of the deposition parameters, series of samples were prepared with only one changing parameter.

From the point of view of the Raman spectra, the most interesting series were those in which the structure changed from fully amorphous to fully microcrystalline. It should be noted that the samples grown close to the amorphous / microcrystalline boundary in the deposition space often exhibit optimum properties regarding the application in solar cells [4] [24] (figure 6.2).

Special samples were also used, in which the crystallinity varied with a position. The reason for the changing structure was either the position of the sample in the deposition chamber or a local inhomogeneity of plasma introduced by a permanent magnet underneath the substrate during the deposition.

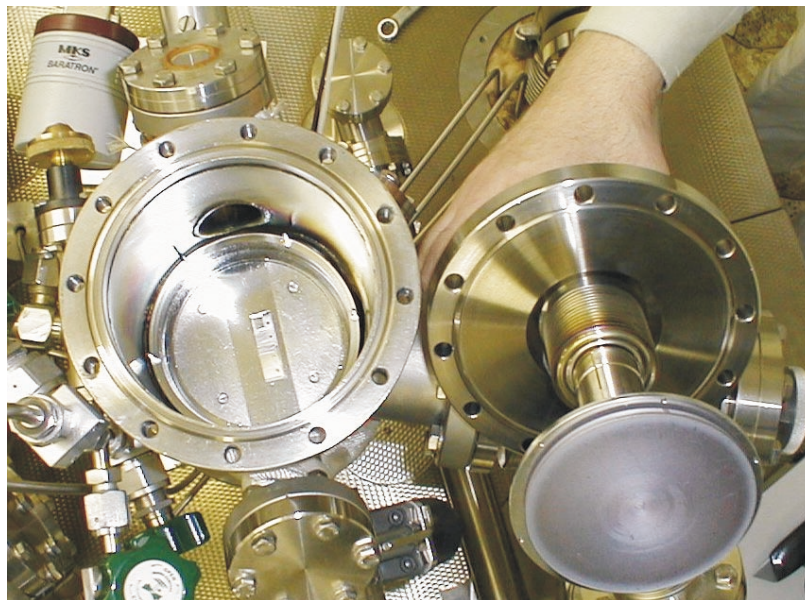
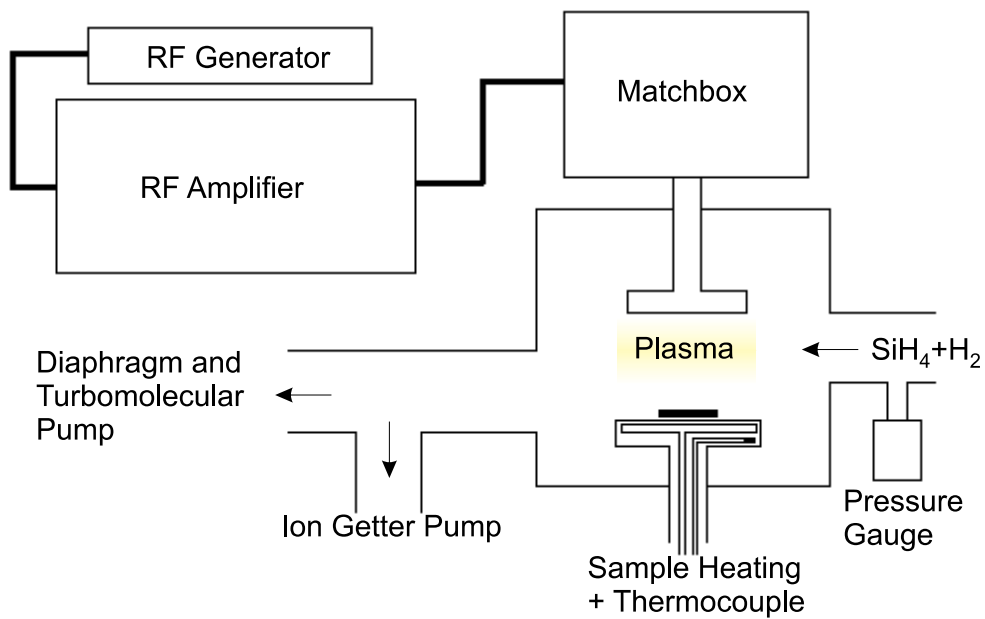


Figure 6.1: The scheme of the PECVD deposition chamber in the laboratory of the Academy of Sciences and a picture of it. The silane or silane diluted in hydrogen is decomposed in plasma discharge and a silicon thin film grows on the substrate, which can be heated. The byproducts are pumped out using the turbomolecular pump and ion getter pump.

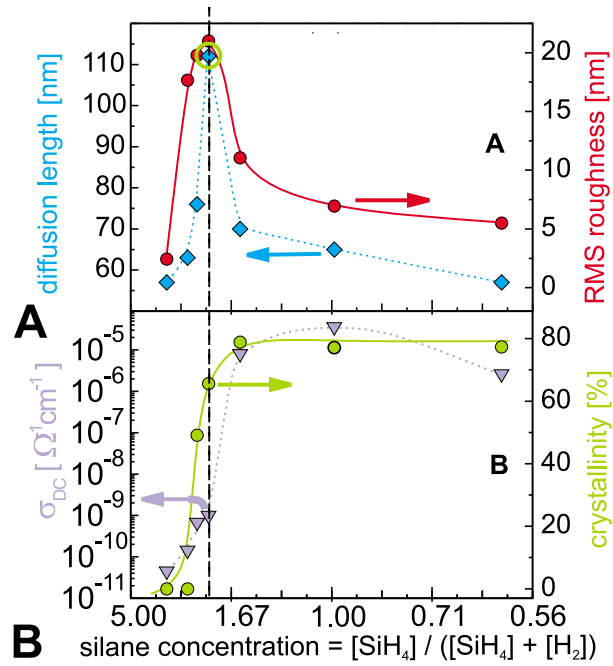


Figure 6.2: Surface roughness and diffusion length L from the steady state photocarrier grating (A) and crystallinity together with dark conductivity σ_{DC} (B) of protocrystalline silicon films of the Manabu Ito dilution series as a function of the silane dilution ratio r_H ranging from 34 to 167. The lines are added as guides for the eye. The best electrical and optical properties are near the percolation threshold, where the crystalline grains which grows from the amorphous tissue starts to connect. The roughness of such microcrystalline material and the diffusion length are also maximal [4].

6.1 Different Series of Samples

6.1.1 The 54 MHz Dilution Series at Temperature of 80°C

This series was made by Mr. Manabu Ito in the Japanese company Toppan Printing by a PECVD on glass substrates (figure 6.3).

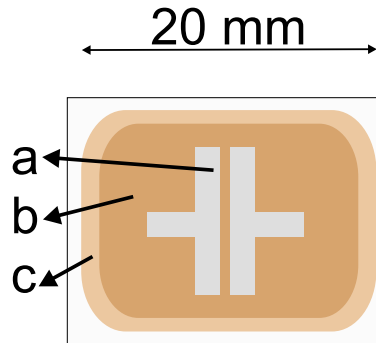


Figure 6.3: The scheme of the typical Manabu Ito sample. Raman spectra are measured in the homogenous part of the sample (b), (c) is an inhomogeneous part on the sample and (a) are contacts.

The flow ratio of hydrogen to silane (so called r_H factor) varied from 26 to 167 and series from amorphous to microcrystalline silicon samples was created. All samples were deposited on a glass *Corning C7059* substrate, the deposition temperature was 80 °C and the frequency of the plasma excitation was set to 54 MHz. The plasma power density was set to ~ 0.35 W/cm². The low deposition temperature was selected to obtain information about the thin film optical and electrical properties, because of the future suitable use of the PET plastics as a substrate material. This series will be referred to as the Manabu Dilution Series (MDS). Table 6.1 contains more details on the deposition parameters of MDS. The deposition duration was adjusted to achieve the thickness of all samples of approximately 1000 nm. The pictures of the MDS made by the AFM microscope are presented in the figure 6.4

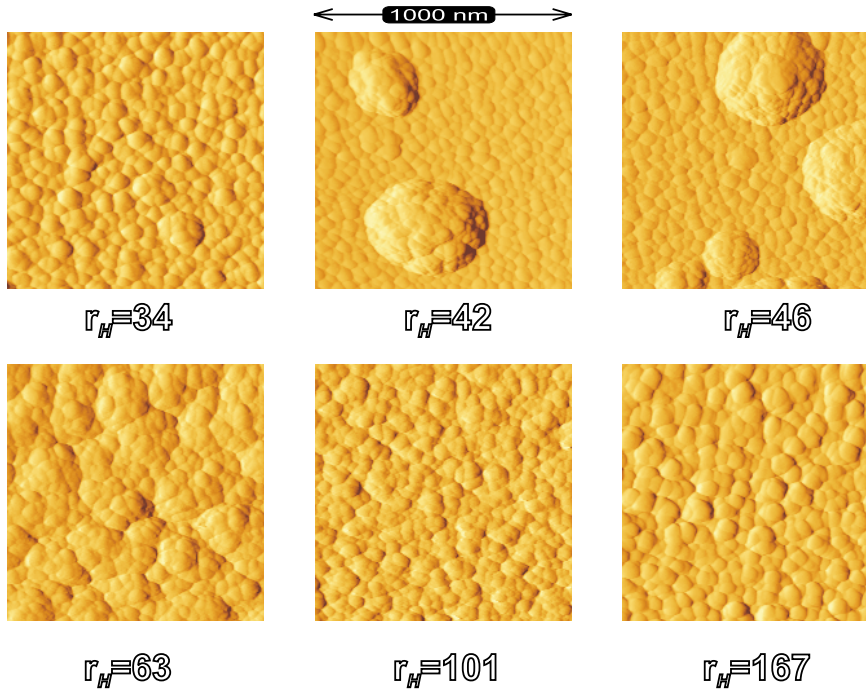


Figure 6.4: The AFM pictures of the Manabu dilution series with the field of view of $1000 \text{ nm} \times 1000 \text{ nm}$ [4].

Table 6.1: Overview of the main deposition parameters of the samples of the Manabu dilution series.

Sample	d [nm]	dil. r_H	power [W]	p_{tot} [Pa]	$[H_2]$ [sccm]	$[SiH_4]$ [sccm]	r_D [nm/s]
010425-1i (MDS 26)	1000	26	10	20	50	1.9	0.33
010425-1i (MDS 34)	1340	34	10	20	50	1.5	0.25
010425-1i (MDS 36)	950	36	10	20	50	1.4	0.24
010425-1i (MDS 39)	910	39	10	20	50	1.3	0.22
010510-2i (MDS 42)	930	43	10	20	50	1.2	0.19
010511-4i (MDS 46)	1000	46	10	20	50	1.1	0.19
010426-1i (MDS 63)	1530	64	10	20	50	0.8	0.17
010425-2i (MDS 101)	1010	101	10	20	50	0.5	0.09
010426-2i (MDS 167)	870	168	10	20	50	0.3	0.06

6.1.2 The Manabu Ito Temperature Series

In this series, deposition of silicon thin films at substrate temperatures from 35 °C to 200 °C was studied using temperature series of samples crossing the boundary between the microcrystalline and amorphous growth. The series of Si samples was deposited by PECVD with the discharge frequency of 54 MHz at the power of 20 W in a mixture of silane and hydrogen with the input pressure of 50 Pa. This series was deposited at substrate temperatures T_S ranging from 35 °C to 200 °C and the dilution ratio $r_H = 133$. All layers were prepared with the thickness around 0.35 μm by adjusting the deposition duration according to the deposition rate at the given T_S . The average deposition rate was $r_D = \sim 0.06$ nm/s and the plasma power density was set to ~ 0.71 W/cm². Main deposition parameters of the samples are summarized in Table 6.2. The pictures of the MTS made by the AFM microscope are presented in the figure 6.5

Table 6.2: Overview of the main deposition parameters of the samples of the Manabu temperature series

Sample	d [nm]	dil. r_H	T_S [°C]	$[H_2]$ [sccm]	$[SiH_4]$ [sccm]
011130-1i (MTS 35)	520	133	35	80	0.6
011130-2i (MTS 50)	300	133	50	80	0.6
011221-1i (MTS 60)	450	133	60	80	0.6
011221-2i (MTS 65)	380	133	65	80	0.6
011221-3i (MTS 70)	380	133	70	80	0.6
011225-1i (MTS 75)	360	133	75	80	0.6
020109-1i (MTS 80)	340	133	80	80	0.6
011220-4i (MTS 85)	290	133	85	80	0.6
011220-3i (MTS 90)	290	133	90	80	0.6
011219-1i (MTS 100)	260	133	100	80	0.6
011219-2i (MTS 110)	300	133	110	80	0.6
011126-4i (MTS 120)	350	133	120	80	0.6
011126-1i (MTS 200)	400	133	200	80	0.6

Note:

The names of the samples have been simplified in our laboratory from the original version indicating the date of the deposition into more understandable name including the value of the key variable parameter (in this case – the substrate temperature) and the abbreviation MTS stands for: **Manabu Ito – Temperature Series**. Then it is clear that the sample MTS 120 denotes the sample of the temperature series prepared at $T_S=120^\circ C$.

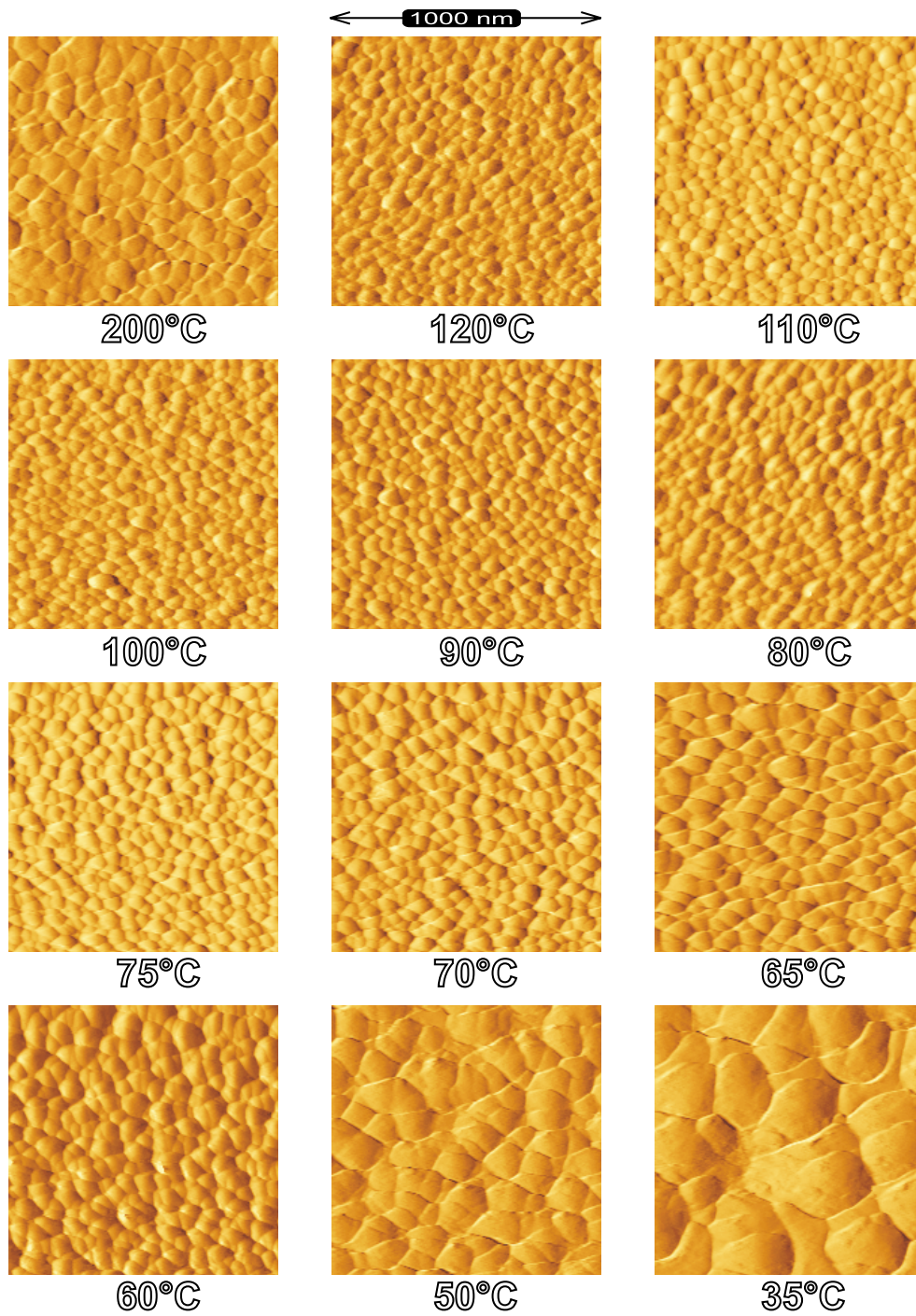


Figure 6.5: The AFM pictures of the Manabu temperature series with the field of view of $1000 \text{ nm} \times 1000 \text{ nm}$ [4].

6.1.3 The STM RF Temperature Series

This series of silicon thin films at low substrate temperatures was prepared by the radio frequency (RF) plasma discharge with the aim to clarify some questions arising from the results of the previous very high frequency temperature series (STM means that these samples were prepared in our deposition chamber, which is connected to STM-AFM microscope embedded in ultra high vacuum chamber). The variable deposition parameter – temperature – again caused the crossing of the boundary between microcrystalline and amorphous growth. The scheme of the typical STM sample is shown in the figure 6.6.

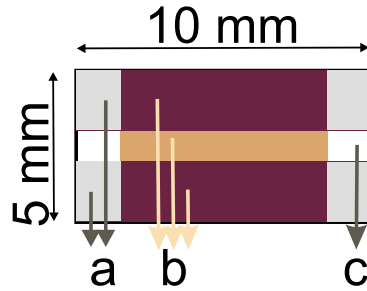


Figure 6.6: The dimensions of the typical STM sample are 5 mm \times 10 mm. The thin silicon film (b) grows on a glass or plastic substrate on which there are NiCr bottom electrodes (a). Between the electrodes is a gap (c), which is approximately 1 mm wide. The Raman measurements are performed in the gap region.

The conventional PECVD parameters were used. This means the discharge at radio frequency of (RF) 13.56 MHz, power around 8.5 W and a mixture of silane and hydrogen with the total pressure of 70 Pa. This series was deposited on the glass substrate at the substrate temperatures T_S ranging from 40 °C to 250 °C and the dilution ratio $r_H = 32$. All the layers were prepared with the thickness around 1 μm by adjusting the deposition time. The main deposition parameters of the samples are summarized in Table 6.3. The average deposition rate was $r_D = \sim 0.08$ nm/s and the plasma power density was set to ~ 0.21 W/cm². The pictures of the STM RF temperature series made by the AFM microscope are presented in the figure 6.7

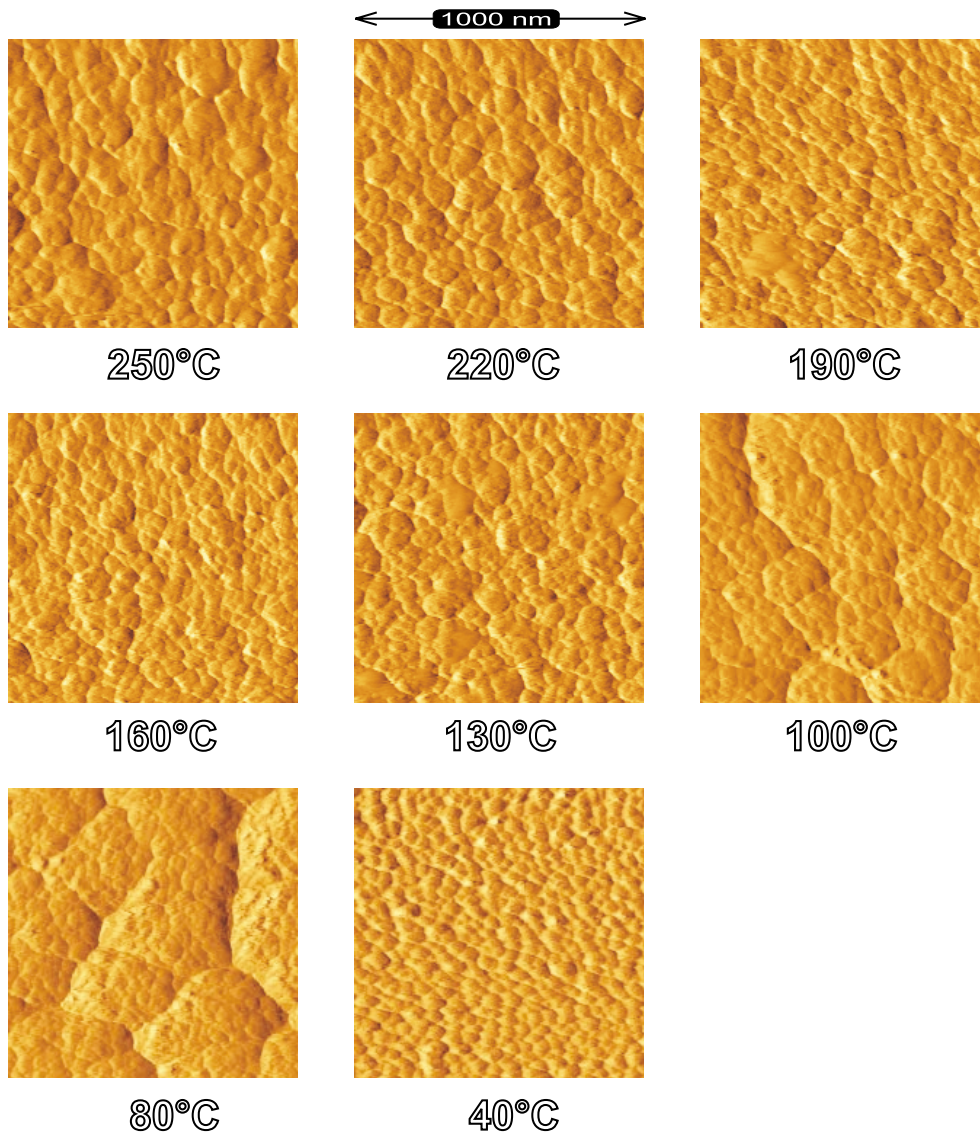


Figure 6.7: The AFM pictures of the STM RF temperature series with the field of view of $1000 \text{ nm} \times 1000 \text{ nm}$ [4].

Table 6.3: Overview of the main deposition parameters of the samples of the STM RF temperature series

Sample	d [nm]	dil. r_H	T_S [°C]	$[H_2]$ [sccm]	$[SiH_4]$ [sccm]
Stm 232	900	32	250	50	1.6
Stm 233	900	32	220	50	1.6
Stm 235	850	32	190	50	1.6
Stm 236	900	32	160	50	1.6
Stm 237	900	32	130	50	1.6
Stm 238	850	32	100	50	1.6
Stm 246	900	32	80	50	1.6
Stm 241	850	32	60	50	1.6
Stm 242	850	32	40	50	1.6

Chapter 7

Results

The Raman spectra presented in this chapter are selected from a much larger set of measurements to illustrate main results of this thesis. They are organized according to our main goal, i.e., finding a practical procedure for evaluating the crystallinity of mixed phase silicon films. During the search we have noticed some common features of the spectra which led us to formulate the following hypotheses:

The amorphous samples: The amorphous samples made under different deposition conditions have approximately the same shape of the spectrum.

The amorphous part of the microcrystalline samples: As the amorphous part of the microcrystalline samples has approximately the same shape as the shape of the fully amorphous spectrum it is possible to subtract the amorphous part of the spectrum, which implies that only fully microcrystalline phase part of the spectrum remains.

The microcrystalline phase: The spectra of the microcrystalline phase can be fitted with two Gaussian curves and a relationship between the parameters of these two Gaussian curves exists (parameters are correlated). (hypothesis formulated in the previous diploma [16])

7.1 Amorphous Samples

The decomposition of the microcrystalline Raman spectrum to the amorphous part of the spectrum and the crystalline part of the spectrum can start by studying only the pure amorphous spectra. In these spectra the key to the decomposition can be found.

Different older amorphous silicon samples were re-measured with the idea of obtaining amorphous samples spectra from samples prepared under different deposition conditions. The main deposition parameters of the samples are summarized in Table 7.1. The sample MHP was prepared by Mr. Manabu Ito and it is the first of the next dilution series made under high pressure. The sample Stm108 was microcrystalline, but it was composed of amorphous parts and crystalline grains and it was possible to obtain the Raman spectrum from the fully amorphous part. The deposition parameters of other amorphous samples which are a part of other series were discussed in the previous chapter where the series were discussed.

Table 7.1: Overview of the main deposition parameters of the amorphous samples

Sample	d [nm]	dil. r_H	T_S [°C]	f_{exc} [MHz]	power [W]	p_{tot} [Pa]
Stm 108	1120	32	250	13.56	19.0	70
Stm 202	1000	12	250	13.56	9.0	70
Stm 211	900	12	250	13.56	9.0	70
Stm 212	1000	0	250	13.56	2.5	70
MHP	292	25	50	54.00	5.0	266
1466M	1000	32	100	13.56	9.0	70
1466R	1000	32	100	13.56	9.0	70

We studied amorphous spectra of samples prepared by PECVD method under different deposition conditions. Some of these samples were prepared in different laboratory (Japan) or in our laboratory in different deposition chambers (1466M, 1466R). The measured Raman spectra are shown in the figure 7.1 A. In the table 7.2 the measurement conditions are presented. The figure 7.1 B shows that the different deposition parameters such as the deposition temperature, type of the substrate, dilution, pressure in the deposition chamber or power of the plasma have only a small impact on the resulting shape of the Raman spectra.

7.2 Fitting the Amorphous Spectra

The idea that the shape of the amorphous part of the spectra is approximately the same for all amorphous samples implies that the amorphous part of the spectrum can also be the same for microcrystalline samples. This can be the crucial information for the decomposition of the microcrystalline spectrum to

Table 7.2: Overview of the main measurement conditions of the amorphous samples

Sample	Laser power [%]	Laser spot radius [μm]	Exposure time [s]
Stm242	10	1	500
Stm202	10	1	500
Stm211	10	1	250
Stm212	10	1	250
Stm2541a	10	1	250
Stm2542a	10	1	250
Stm282-8	50	10	250
1466M	10	1	250
1466R	10	1	250
Stm108	100	10	250
MHP	50	10	250
MDS 26	50	10	250
MDS 34	50	10	250
MDS 36	50	10	250
MDS 39	50	10	250

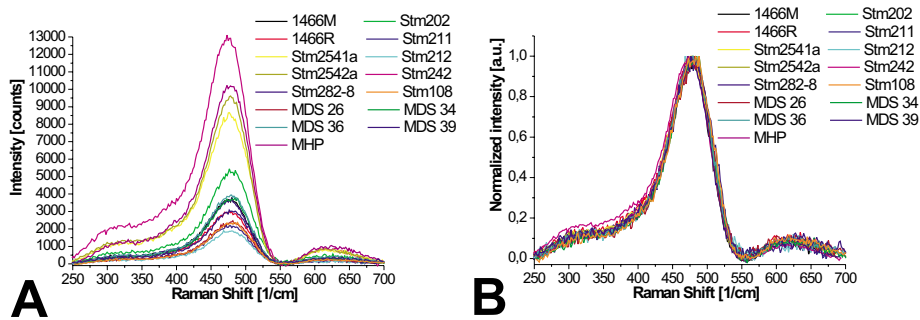


Figure 7.1: In the figure A the raw spectra of amorphous samples are presented. Spectra with normalized amplitude to one are shown in the figure B.

the amorphous part and the crystalline part (it can be done in the program DOORS after pressing the *Subtract Amorph* button from the main menu).

The amorphous spectrum is composed of the LO phonon, LA phonon and TO phonon bands. For obtaining the pure amorphous TO phonon signal we tried to fit the amorphous spectra. Assuming that the amorphous spectra are approximately all the same, we have fitted the best measured spectrum

(Stm242) which has the smallest error of the data measured.

According to [8] [25] the maximum of the LO phonon is centred at 380 cm^{-1} and the LA phonon, is centred at 310 cm^{-1} . We have fitted the amorphous spectrum with three Gaussians. The first one had the position of the centre fixed at 310 cm^{-1} and the second at 380 cm^{-1} . The third Gaussian did not have any parameters fixed. In the figure 7.2 A it is shown that this is not the best way to obtain the TO amorphous signal. If we let all the parameters free in the fitting process, the Gaussian which represented the LA amorphous phonon will shift its centre to higher wavenumbers (419 cm^{-1}). Our next trial was to fit the spectrum with two Gaussians for TO phonon instead of one Gaussian (figure 7.2 B). The black line, which is the sum of all Gaussians (first for LA phonon, second for LO phonon and the rest for TO amorphous phonon) in the figure, describes now the spectrum well.

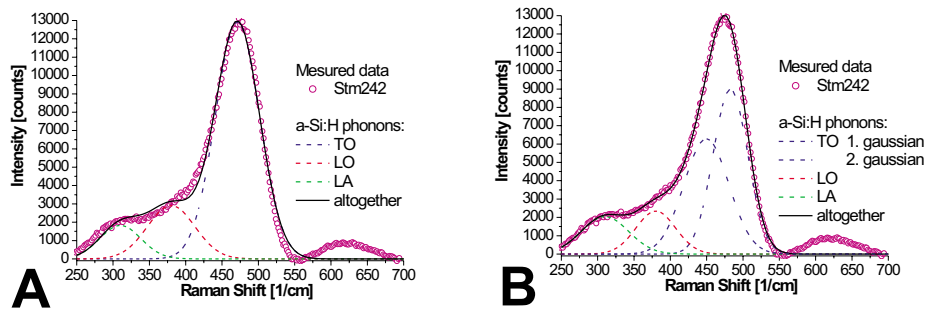


Figure 7.2: In the figure A the fitting of the best measured amorphous spectrum (sample Stm242) fitted with three Gaussian is presented. The same spectrum is in the figure B with four Gaussians fitted. The blue dashed line represent the amorphous TO phonon, the red dashed line represents the LO amorphous phonon (fixed position of the centre at 380 cm^{-1}), and finally the green dashed line represents the LA amorphous phonon (fixed position of the centre at 310 cm^{-1}). The black solid line is the sum of all Gaussians.

7.3 Fitting the Microcrystalline Spectra

The fully microcrystalline phase of the spectrum which is presented by the crystalline TO phonon can be obtained by subtracting the amorphous spectrum multiplied with an amplitude (adjusted to fit the data) from microcrystalline spectrum.

The Gaussian curve has three parameters: the amplitude, the centre and the width. Describing the fully microcrystalline phase signal with two Gaus-

sians, six parameters are needed. If there is a physical reason for the fact, that this shape is well described by two Gaussians, the dependance between the parameters of these functions must exist. In our further discussion we will concentrate on finding such relations. The proper parameters, which should show this kind of relations between two Gaussians could be the difference of their centres, the ratio of their amplitudes and the ratio of their widths. Such a function, having first three parameters of normal Gaussian and other three parameters like these, creating the second Gaussian curve was built-in into our program DOORS (*UAmorf* function).

If we know the areas of the amorphous and crystalline TO phonons, the crystallinity can be computed using the equation (2.8). The area of the crystalline TO phonon can be gained using the previous procedure, but the pure signal of the TO amorphous phonon is difficult to obtain.

Let's assume that the amorphous part of the spectrum is the same also in the microcrystalline spectrum, only it is multiplied with an amplitude (a constant value for all points of the spectrum). Neglecting for a moment the TA and LA amorphous phonon bands, because of their small signal, the amorphous spectrum is approximated with two Gaussians representing the TO amorphous phonon (figure 7.3 A). If we multiply this "amorphous" spectrum with a constant value for each point (figure 7.3 B), all the TO Gaussians parameters stay the same, only the amplitudes of Gaussians will be multiplied with this constant value. As both the amplitudes were multiplied with the same constant value, the ratio between them stays the same as it was before multiplying. The result of this "amorphous" multiplying is fact, that doing the manual subtracting by multiplying the amorphous spectrum is the same procedure as fitting the microcrystalline spectra with two TO Gaussians with constant ratio of their amplitudes, constant ratio of their widths and constant position of their centres. Such a function is described with the function *UAmorf*. The one and the only parameter of this function, which changes at fitting the microcrystalline spectrum, is the amplitude, the rest of the *UAmorf* parameters stays fixed.

How should the fitting of the microcrystalline silicon spectrum look like? First, the pure amorphous spectrum has to be fitted. As a result of this fit the parameters describing the TO, LA and LO phonons are obtained. Afterwards, we can fit the microcrystalline spectra with the *UAmorf* function for the TO amorphous phonon using the obtained parameters of the TO phonon from the amorphous spectrum except for the amplitude. The amplitude will be fitted whereas all other parameters, including the amplitude ratio, will be fixed. The LA and LO phonons can be fitted with two Gaussians, again with the parameters obtained from the amorphous spectrum. Two methods can be used: either fixing all the parameters except for both amplitudes, or keeping

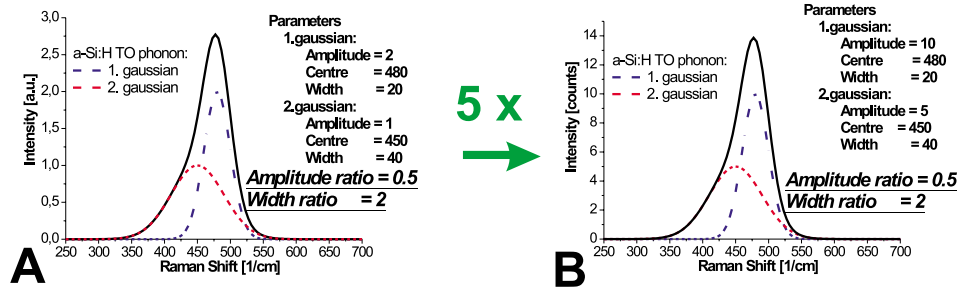


Figure 7.3: An imaginary spectrum of the TO amorphous phonon composed of two Gaussians (A) is multiplied by the factor of 5 (B). The ratio of the amplitudes and the ratio of the widths stays constant.

the ratio of the amplitudes constant. The latter case corresponds to the fitting with the UAmorf function. As the contribution of LA and LO phonons is small, by not fixing their amplitudes ratio the effect on TO amorphous Gaussians will be minimal. The TO crystalline phonon can be fitted using two Gaussians curves, or the UAmorf function with no parameters fixed. We will refer to this procedure as a microcrystalline **UAmorf-amorph** fitting.

This simple procedure allows us to decompose the microcrystalline spectrum and gain the areas of the amorphous and crystalline TO phonons, which are crucial for the crystallinity evaluation.

7.4 Series of the Nucleation Density on the Sample Stm282

In our laboratory a special sample named Stm282 was prepared. A permanent magnet was placed under the sample in the deposition chamber (figure 7.4).

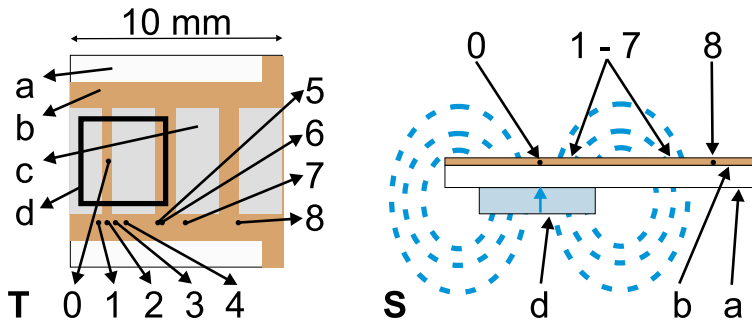


Figure 7.4: The **T**-top and the **S**-side view of scheme of the Stm282 sample. The thin silicon film (b) grows on the plastic substrate (a). On the top of the film are electrodes (c). The square (d) shows a position of the permanent magnet. The numbers 0–8 are points where the measurements were performed.

The magnetic field influenced the trajectories of the charged particles in the plasma and increased the nucleation density in some positions of the sample (positions 1–7 in the figure 7.4), which were near the edges of the placed permanent magnet. The nucleation density was probably increased by the improved ionization of the silane radicals caused by the collisions with electrons trapped in the "magnetic tunnel". Similar effect is used in the magnetrons in the sputtering machines. The orientation of the magnetic field (lines of force) was perpendicular to the substrate plane (figure 7.4 S). In order to get sufficiently high magnetic field on the surface of the sample, the thin plastic foil (120 μm) was employed as a substrate for the PECVD method. The pictures of the different positions on the sample Stm282 with different nucleation density series made by the optical microscope are presented in the figure 7.5.

Table 7.3: Overview of the main deposition parameters of the sample Stm282

Sample	d [nm]	dil. r_H	T_S [$^{\circ}\text{C}$]	f_{exc} [MHz]	power [W]	p_{tot} [Pa]
Stm282	600	32	100	13.56	9.0	70

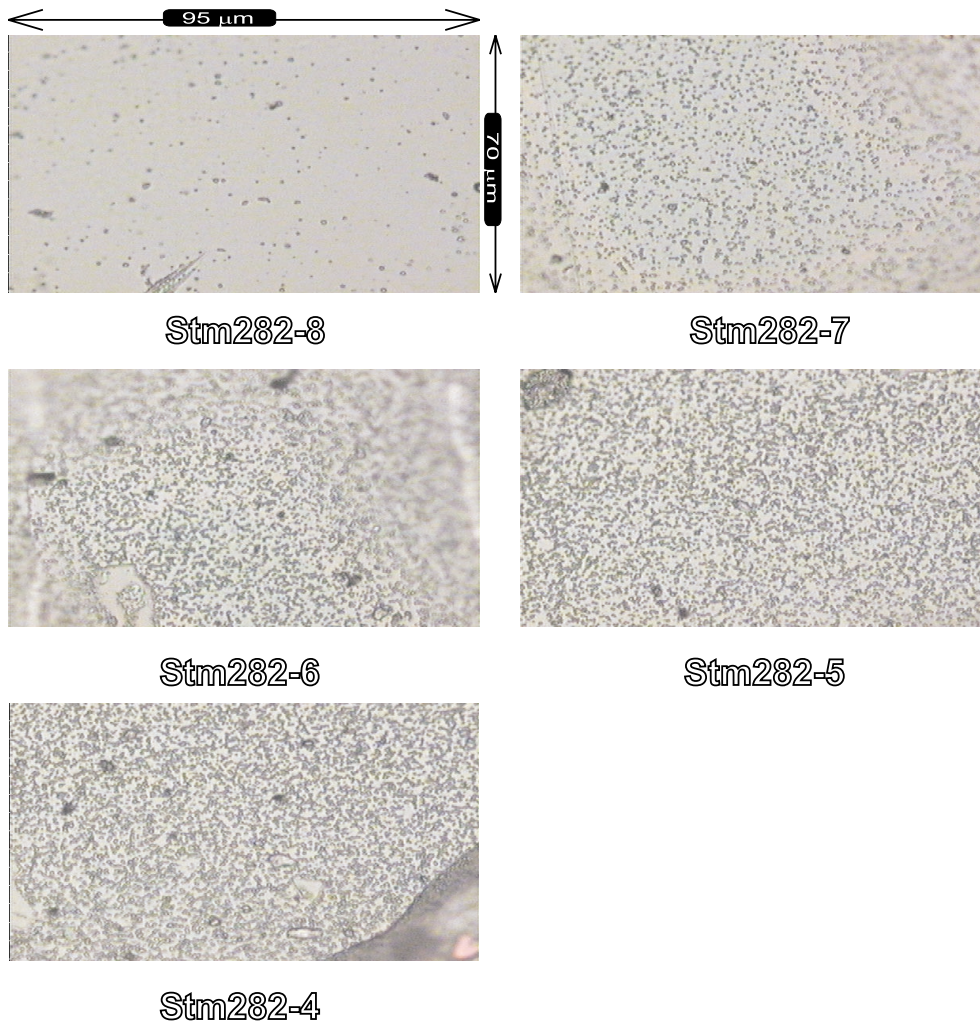


Figure 7.5: The pictures of the Stm282 nucleation density series made by the optical microscope with the field of view of $95 \mu\text{m} \times 70 \mu\text{m}$.

From the microscope images (shown in the figure 7.5) made in different distances from the edge of the sample it is evident that the crystalline grains are approximately of the same dimension, only their density varies. The nuclei density and also the signal from the crystalline part of the sample decrease as the distance from the edge of the magnet increases. In the part of the sample, where approximately the centre of the magnet was placed, the Raman spectrum of the sample was amorphous. The Raman spectra were measured on sample as shown in the figure 7.4.

The spectra Stm282-1 and Stm282-7 were very similar to each other as spectra Stm282-3 and Stm282-4 were. It was possible to create a series of

the spectra Stm282-4, Stm282-5, Stm282-6, Stm282-7 and Stm282-8, where nucleation density and the signal from the crystalline part of the sample decrease as a function of the distance from the edge of sample. The measurement conditions are presented in the table 7.4. The exposure time was for all samples set to 250 s.

Table 7.4: Overview of the sample Stm282 measurement conditions.

Sample	Laser power [%]	Distance from the edge [mm]	Laser spot radius [μm]	Note
Stm282-0	10	1.7	1	amorph., magnet centr.
Stm282-1	50	1.4	10	similar as Stm282-7
Stm282-2	50	1.8	10	similar as Stm282-6
Stm282-3	50	2.2	10	similar as Stm282-4
Stm282-4	50	2.7	10	similar as Stm282-3
Stm282-5	50	4.2	10	
Stm282-6	50	4.4	10	similar as Stm282-2
Stm282-7	50	5.5	10	similar as Stm282-1
Stm282-8	50	8.0	10	amorphous

The raw Raman spectra are presented in figure 7.6 A. Assuming that the spectrum of the amorphous part of all samples is the same, the signal of the amorphous spectrum Stm282-8 was subtracted, then it was multiplied by an amplitude adjusted to fit the particular data. The crystalline signal which remains after this procedure is shown in the figure 7.6 B. If the crystalline signal is then normalized (7.6 C), it is evident that the crystalline spectrum has the same shape for all microcrystalline spectra.

The shape of these crystalline signals from locations with different nucleation densities is very similar. This fact is confirmed by the decomposition of the normalized crystalline signals to the sum of two Gaussians (figure 7.7 A). The two Gaussians (dashed lines) and the sum of these two curves (solid line) are of the same colour for each spectrum. As the fully microcrystalline phase signal is asymmetric and two Gaussians can describe this shape of the spectra well and other laboratories report on fitting this crystalline peak with the same curves [22], we also decided to describe the crystalline signal with two Gaussians. The centres of the fitted Gaussians are shown in the figure 7.7 B. According to the figure 7.7 A, the first Gaussian is taller and narrower (the first crystalline peak) and the second one, positioned at lower wavenumbers, is smaller and broader (the second crystalline peak).

Subtracting the amorphous part manually may insert an error to remaining fully microcrystalline phase spectrum. The better way to do this

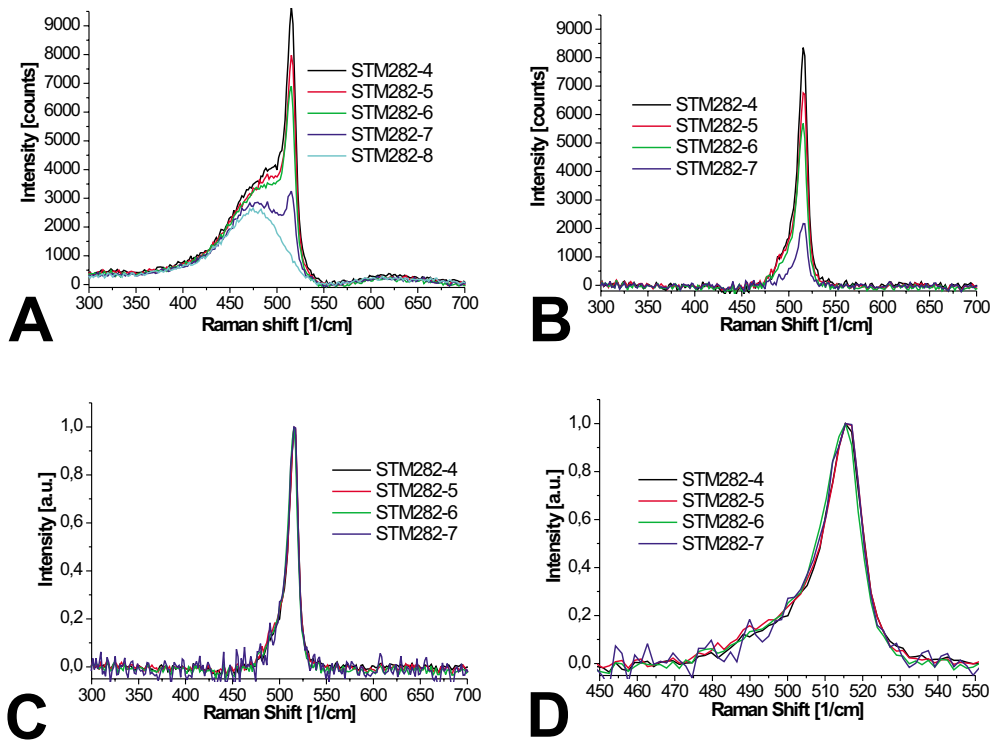


Figure 7.6: In the figure A the raw spectra of the sample *Stm282* are presented. Afterwards the amorphous spectrum multiplied with an amplitude (adjusted to fit the data) was subtracted, the crystalline part of the spectra remained (B). Then the amplitude of the signal was normalized (C) and the detailed part of the spectrum is showed in the figure (D).

subtraction is to fit the whole microcrystalline spectrum with the functions representing the amorphous part and the function representing the fully microcrystalline phase.

Using the $\mu c - UAmorf - amorph$ procedure all the microcrystalline *Stm282* spectra chosen to *Stm282* nucleation density series were fitted. The comparison between the results of the fitting by this procedure and the results obtained by fitting the manually subtracted amorphous part of the spectra are shown in the figure 7.8. The difference of widths obtained by these methods is very small (figure 7.8 A). The ratio of the amplitudes of the first to second crystalline peak is showed in the figure 7.8 B and they are also similar. The similarity can be seen in the figure 7.8 C too, where the difference of Gaussians positions is presented. In the last figure the ratio between widths of the broader and less broader crystalline peak is presented.

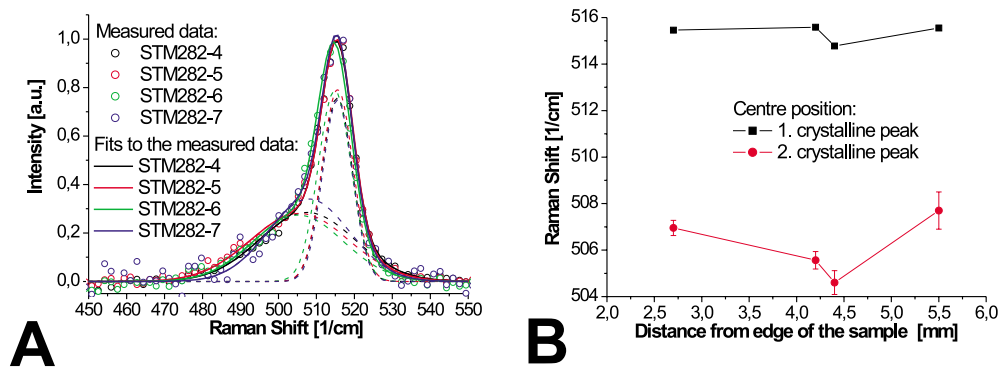


Figure 7.7: The normalized crystalline part of the spectra of the sample *Stm282* was fitted with two Gaussians (A – dashed lines of the same colour as the spectrum are two Gaussians and the solid lines are their sums). The positions of centres as a function of the distance from the edge of the samples are shown in the figure B.

According to the errors, both methods gives the same results.

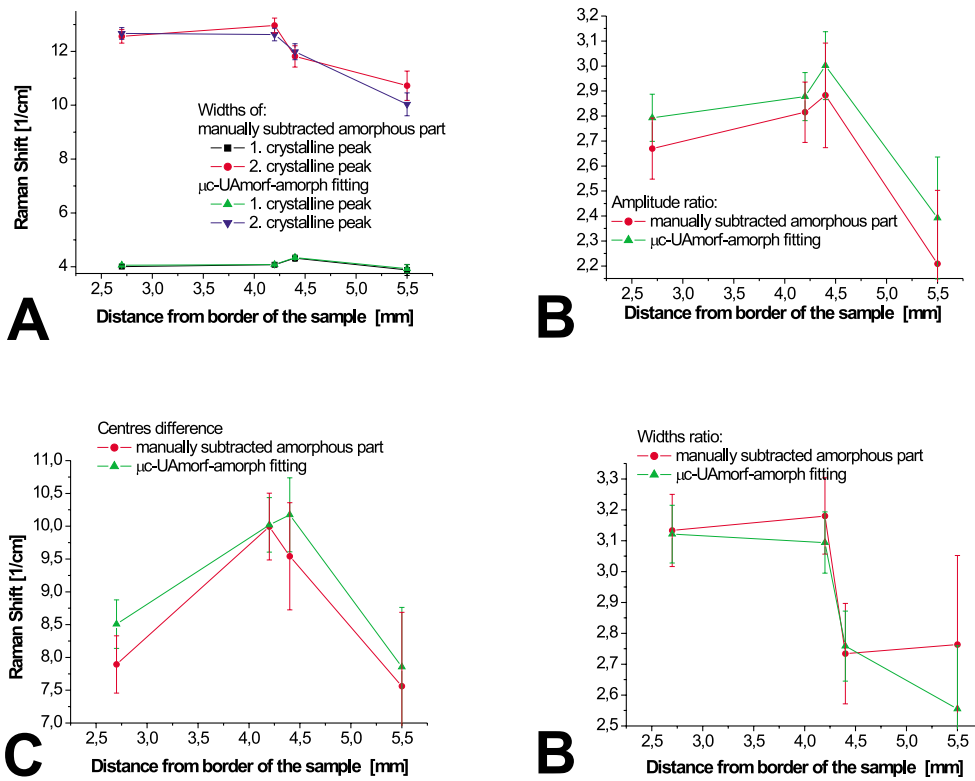


Figure 7.8: The widths of crystalline peaks of the sample *Stm282* fitted with $\mu\text{C} - \text{UAmorf} - \text{amorph}$ method or fitted only crystalline peaks obtained by manually subtracting the amorphous part of the spectra are shown in A. The ratio of crystalline amplitudes (B), the difference of crystalline centres (C) and the ratio of crystalline widths (D) are similar for both used methods.

7.5 Nucleation Density on the Samples Stm254

Other samples, where the plasma changed the nucleation density and also the crystallinity, are in the Stm254 samples (Stm2541, Stm2542, Stm2543) which were deposited in one deposition.

This information was gained during this thesis after re-measuring the samples Stm254 by an AFM microscope, because of the similar plasma inhomogeneity deposition parameter as by the deposition of the sample Stm282.

As our round shaped plasma electrode creates an inhomogeneous plasma, the crystallinity of the samples is different not only for different samples, but also for different positions on the substrate holder of one sample. This dependance is not a simple function of the distance from the centre of the electrode. According to this fact, a series of spectra with increasing crystallinity resulting from single deposition was created. In the centre of the deposition chamber, where the plasma is most homogenous and where the sample Stm2542 was placed, the thin film has grown as fully amorphous or as almost fully amorphous. On the edges of the deposition chamber, the samples Stm2541 and Stm2543 has grown as microcrystalline (figure 7.9).

The discharge frequency was set to 13.56 MHz, power around 8 W and a mixture of silane and hydrogen with the total pressure of 70 Pa. The deposition was done at substrate temperatures $T_S \sim 60$ °C and the dilution ratio $r_H = 32$ ($[H_2] = 50$ sccm and $[SiH_4] = 1.6$ sccm). The main deposition parameters of the samples are summarized in the table 7.5. The average deposition rate was $r_D = \sim 0.1$ nm/s and the plasma power density was set to ~ 0.21 W/cm².

Table 7.5: Overview of the main deposition parameters of the samples of the Stm254 Position Series

Sample	d [nm]	distance [mm]
Stm 2541	850	-20
Stm 2542	700	0
Stm 2543	900	+20

The Raman spectra were measured in three different points of each sample: the left side of the gap, the right side of the gap and the middle of the gap. These three places were named with letters a, b and c. The measurement conditions are presented in the table 7.6 and the pictures of the Stm254 series made by the AFM microscope are presented in the figure 7.10

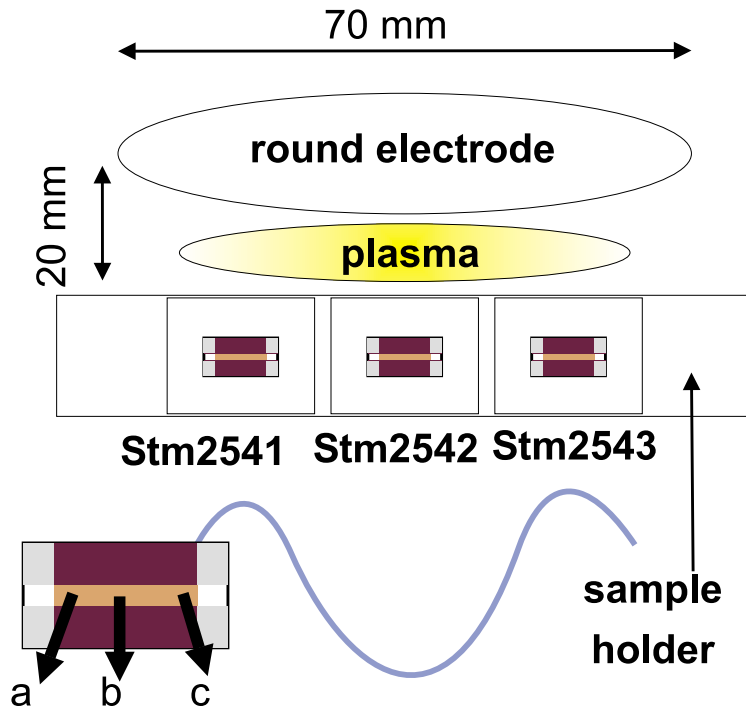


Figure 7.9: The scheme of the deposition chamber with positions of the *Stm254* samples. The blue line approximately shows the crystallinity development. All samples were measured in three different positions on the substrate holder: a, b, c. The round plasma electrode had 70 mm in the diameter and it was placed 20 mm above the samples holder.

Table 7.6: Overview of the main measurement conditions of the *Stm254* series

Sample	Laser power [%]	Laser spot radius [μm]	Exposure time [s]	Note
Stm2541a	10	1	250	similar as Stm2543c
Stm2541b	10	1	250	
Stm2541c	10	1	250	amorphous
Stm2542a	10	1	250	amorphous
Stm2542b	10	1	250	amorphous
Stm2542c	10	1	250	
Stm2543a	10	1	250	similar as Stm2543b
Stm2543b	10	1	250	similar as Stm2543a
Stm2543c	10	1	250	similar as Stm2541a

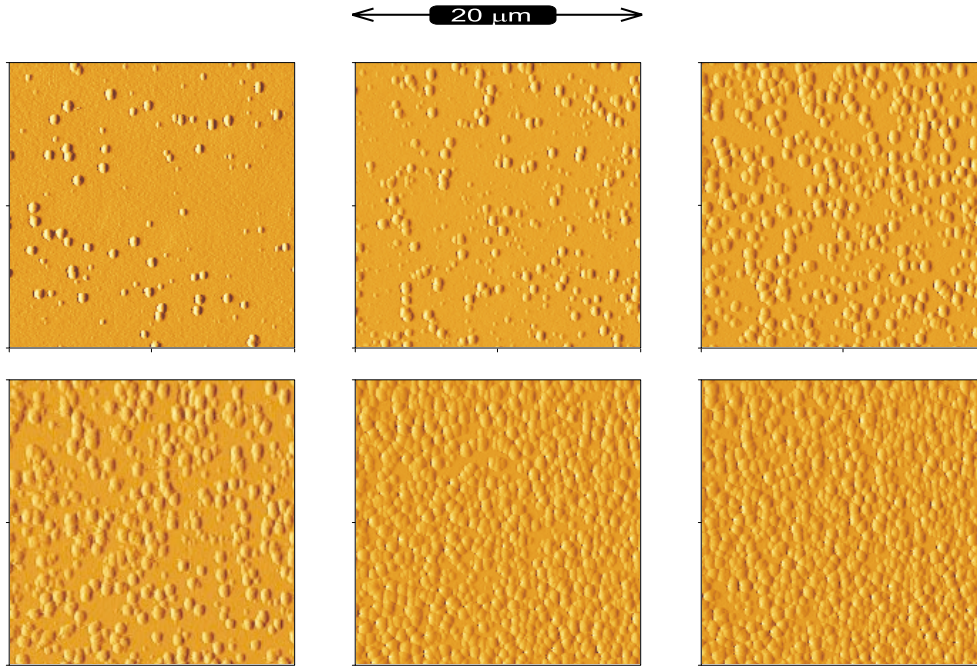


Figure 7.10: The AFM pictures of the *Stm254* position series with the field of view of $20\ \mu\text{m} \times 20\ \mu\text{m}$.

As some of the spectra are very similar only spectra *Stm2542c*, *Stm2543b*, *Stm2543c*, *Stm2541b* and the amorphous spectrum *Stm2542a* create a *Stm254* series (figure 7.11 A). We have manually subtracted the amorphous spectrum *Stm2542a* as described previously (figure 7.11 B). The spectra have been normalized (figure 7.11 C) and detailed look at the spectra is presented in the last figure 7.11 D. According to the figure 7.11 D only the spectrum *Stm2542C*, which is the spectrum with smallest crystalline signal, differs from the very similar shape of the others (normalized) spectra. Comparing with distance series *Stm282*, where the plasma inhomogeneity (caused by magnetic field) was also the only one parameter which changes in the deposition chamber, the crystalline spectra have for each series similar shape.

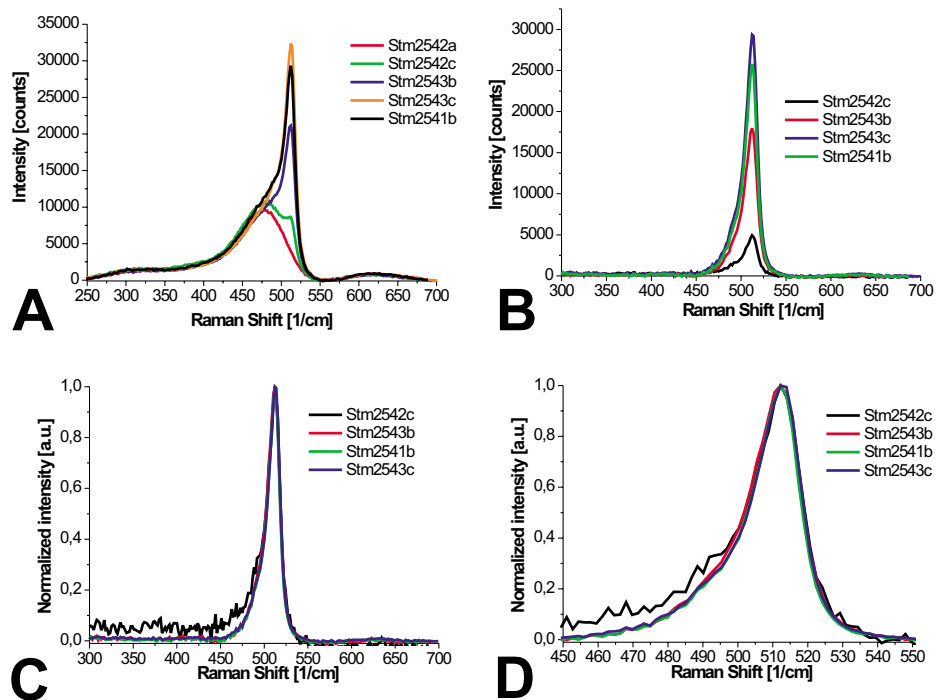


Figure 7.11: In the figure A the raw spectra of the samples Stm254 are presented. After the amorphous spectrum multiplied with an amplitude (adjusted to fit the data) was subtracted, the crystalline part of the spectra remained (B). Then the amplitude of the signal was normalized (C) and the detailed part of the spectrum is shown in the figure (D).

We have fitted the fully microcrystalline phase spectra and the whole microcrystalline spectra (using the $\mu c - UAmorf - amorph$ method). The results of these fits are shown in the figure 7.12.

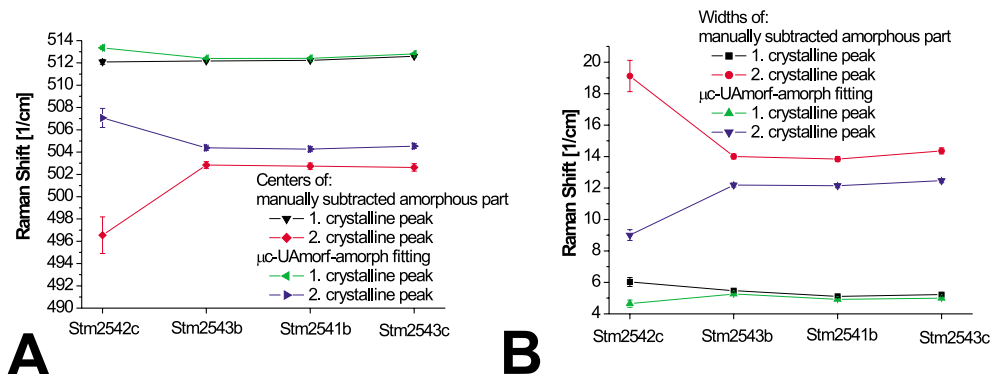


Figure 7.12: The position of centres (A) and the widths (B) of crystalline peaks fitted with $\mu c - UAmorf - amorph$ method or fitted only crystalline peaks obtained by manually subtracting the amorphous part of the spectra of the nucleation density Stm254 series.

Upon a closer look to the figure 7.12 it can be seen that as the spectrum Stm2542c had a smallest crystalline signal, the errors of its fit are the greatest. It is not surprising that the rest of the spectra have very similar values of the positions and widths, because of their similar shapes of spectra (figure 7.11 D).

The same conclusion can be made of the parameters, which can better describe the relations between two Gaussians. The ratio of the amplitudes (figure 7.13 A), the difference of the centres (figure 7.13 B) and the ratio of the widths (figure 7.13 C) of crystalline peaks fitted with $\mu c - UAmorf - amorph$ method or fitted only crystalline peaks obtained by manual subtracting the amorphous part of the spectra are similar for both used methods. The difference can be caused by the error introduced by the manual subtraction of the amorphous part.

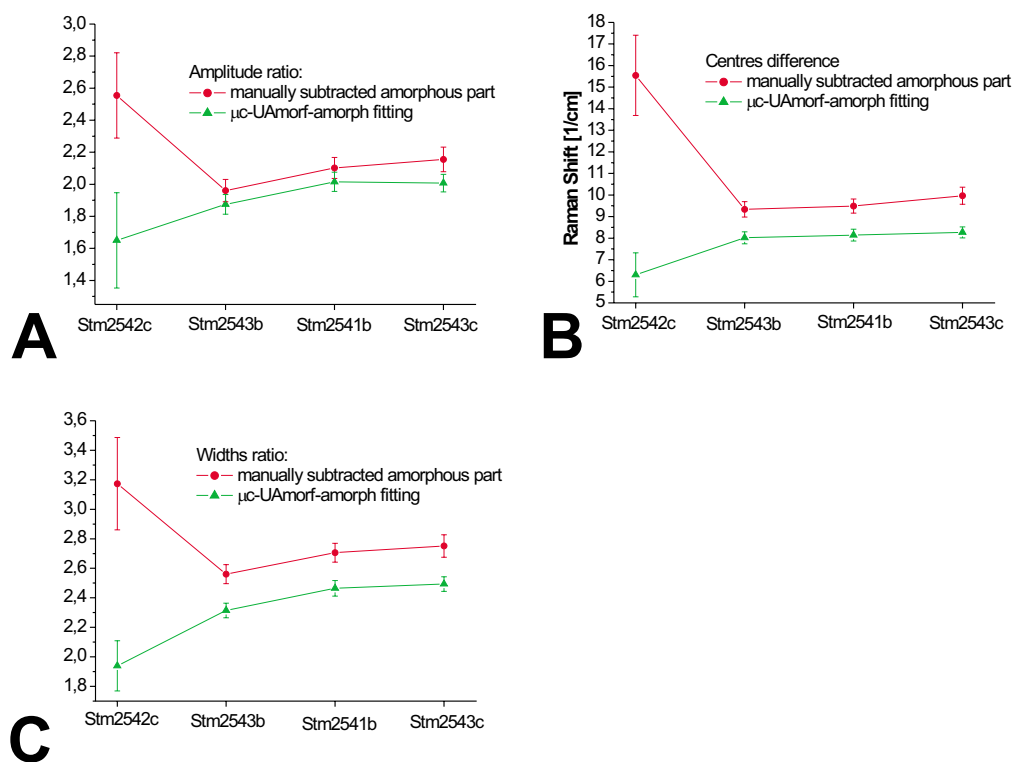


Figure 7.13: The ratio of the amplitudes (A), the difference of the centres (B) and the ratio of the widths (C) of crystalline peaks fitted with $\mu c - UAmorf - amorph$ method or fitted only crystalline peaks obtained by manual subtracting the amorphous part of the spectra of the nucleation density Stm254 series are similar for both used methods.

7.6 Manabu Ito Dilution Series (MDS)

This series was prepared in Toppan Printing laboratory. The series is composed of nine samples. The samples MDS 26, MDS 34, MDS 36 and MDS 39 were fully amorphous and they were already discussed in previous part of this thesis. The rest of the series is composed of microcrystalline samples. The measurement conditions of them are presented in the table 7.7.

Table 7.7: Overview of the main measurement conditions of the Manabu dilution series.

Sample	Laser power [%]	Laser spot radius [μm]	Exposure time [s]
MDS 42	50	10	250
MDS 46	50	10	250
MDS 63	50	10	250
MDS 101	50	10	250
MDS 167	50	10	250

We have manually subtracted the amorphous spectrum MDS 26 as described previously (figure 7.14 B). The spectra have been normalized (figure 7.14 C) and a detailed look at the spectra is presented in the last figure 7.14 D. According to the figure 7.14 D the spectra MDS 42 and MDS 46, which are the spectra with smallest crystalline signals, have slightly different shape of the normalized crystalline spectra. The rest of the series spectra have very similar shapes. The small shift can be caused as a result of the dilution.

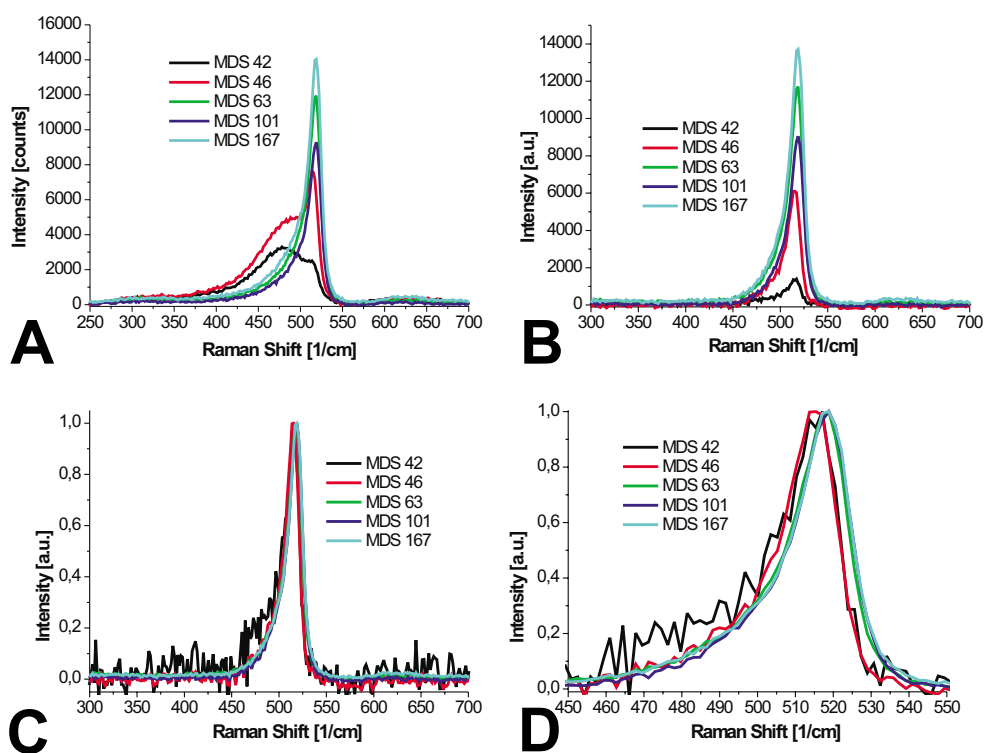


Figure 7.14: In the figure A the raw microcrystalline spectra of the samples of the MDS are presented. Afterwards the amorphous spectrum MDS 26 multiplied with an amplitude (adjusted to fit the data) was subtracted, the fully microcrystalline phase of the spectra remained (B). Then the amplitude of the signal was normalized (C) and the detailed part of the spectra is showed in the figure (D).

We have fitted the fully microcrystalline phase spectra and also the whole microcrystalline spectra (using the $\mu c - UAmorph - amorph$ method). The results of these fits are shown in the figure 7.15.

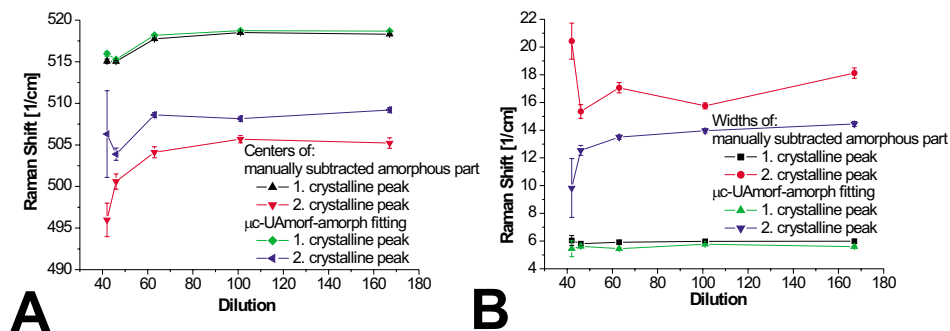


Figure 7.15: The position of centres (A) and the widths (B) of crystalline peaks fitted with $\mu c - UAmorph - amorph$ method or fitted only crystalline peaks obtained by manually subtracting the amorphous part of the spectra of the Manabu dilution series.

Upon the closer look to the figure 7.15 it can be seen that the spectrum MDS 42 has a smallest crystalline signal and the errors of the fit parameters are the greatest. It is not surprising, that the rest of the spectra have similar values of the positions and widths, because of the similar shapes of their spectra (figure 7.14 D).

The same conclusion can be drawn from the parameters, which can better describe the relations between two Gaussians. The ratio of the amplitudes (figure 7.16 A) the difference of the centres (figure 7.16 B) and the ratio of the widths (figure 7.16 C) of crystalline peaks fitted with $\mu c - UAmorph - amorph$ method or fitted only crystalline peaks obtained by manual subtracting the amorphous part of the spectra have similar behaviour for both used methods. The difference can be caused by the error due to using manual subtraction of the amorphous part.

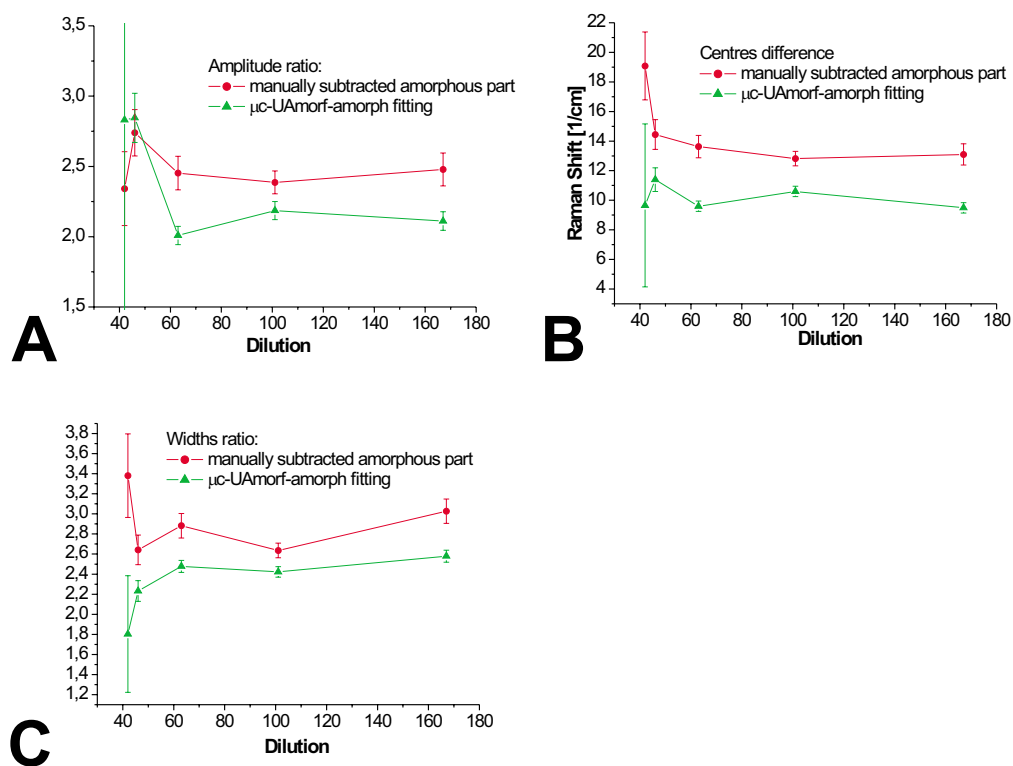


Figure 7.16: The ratio of the amplitudes (A), the difference of the centres (B) and the ratio of the widths (C) of crystalline peaks fitted with μ c - UAmorf - amorph method or fitted only crystalline peaks obtained by manual subtracting the amorphous part of the spectra of the MDS are similar for both used methods.

7.7 Manabu Ito Temperature Series (MTS)

This is another series which was prepared in Toppan Printing laboratory. It is the most detailed series which will be presented in this thesis. It is composed of thirteen microcrystalline samples. Even if the temperature was 35 °C the sample was not amorphous. The measurement conditions of MTS are presented in the table 7.8.

Table 7.8: Overview of the main measurement conditions of the Manabu temperature series.

Sample	Laser power [%]	Laser spot radius [μm]	Exposure time [s]
MTS 35	50	10	250
MTS 50	50	10	250
MTS 60	50	10	250
MTS 65	50	10	250
MTS 70	50	10	250
MTS 75	50	10	250
MTS 80	50	10	250
MTS 85	50	10	250
MTS 90	50	10	250
MTS 100	50	10	250
MTS 110	50	10	250
MTS 200	50	10	250

As the series does not contain an amorphous sample we have manually subtracted the amorphous spectrum of our best measured sample Stm242 as we have previously described (figure 7.17 B). The spectra have been normalized (figure 7.17 C). The shift of the maximum of Raman signal caused by the deposition temperature was found.

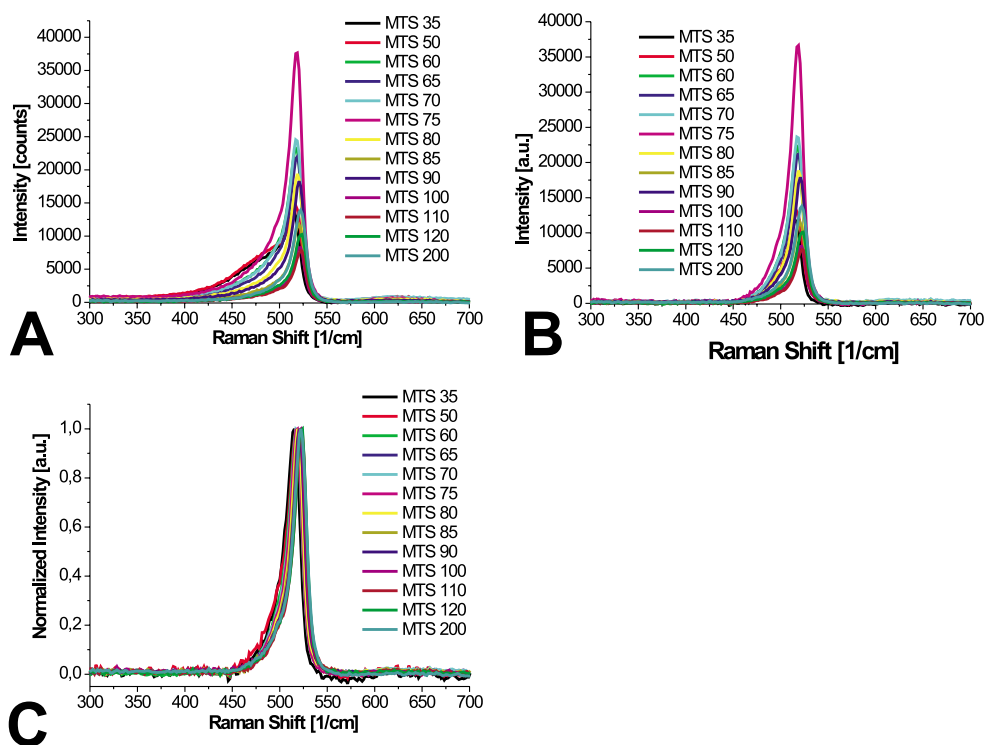


Figure 7.17: In the figure A the raw microcrystalline spectra of the samples of the MTS are presented. Afterwards the amorphous spectrum *Stm242* multiplied with an amplitude (adjusted to fit the data) was subtracted, the fully microcrystalline phase of the spectra remained (B). Then the amplitude of the signal was normalized (C).

For comparing the shape of the pure microcrystalline spectra we have shifted the spectra so that they have the maximum at the same position. The detailed view of the spectra before the shift (A) and after the shift (B) is presented in the figure 7.18. According to the figure 7.18 B the spectra have similar but not exactly the same shape, as we have observed in the previous series.

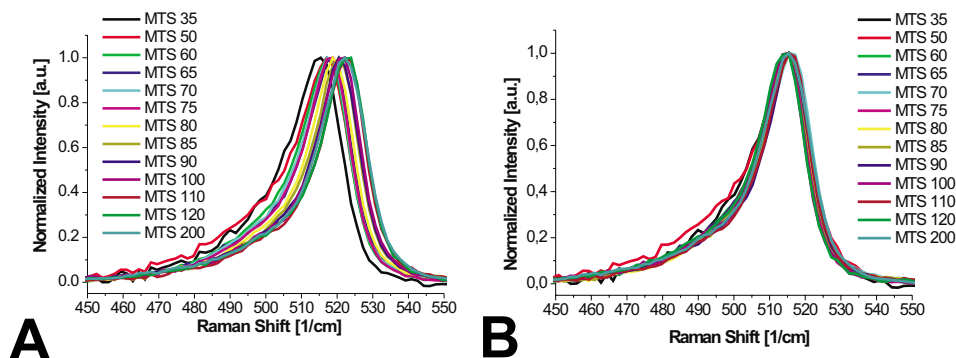


Figure 7.18: The detailed part of the spectra of the MTS before (A) and after (B) the shift of the Raman spectra to the same maximum of the Raman signal.

We have fitted the fully microcrystalline phase spectra (not shifted to the common maximum of the Raman signal) and also the whole microcrystalline spectra (using the $\mu c - UAmorf - amorph$ method). As the maximum of the Raman signal was not the same for spectra of this series, we have also fitted the whole microcrystalline spectra using the $\mu c - UAmorf - amorph$ method, but we have moved and then fixed the centre of the $UAmorf$ function so that the difference of maximum of Raman signal and maximum of the amorphous signal stays constant. The results of these fits are shown in the figure 7.19. The position and width of the second crystalline peak is slightly different using different fitting methods, but their behaviour for the series is very similar.

It is evident from the results of the parameters fitting, which can better describe the relations between two Gaussians, that the microcrystalline spectra of the Manabu temperatures series do not have exactly the same shape. The ratio of the amplitudes (figure 7.20 A) as a function of the temperature increases approximately linearly. The difference of the centres (figure 7.20 B) stays approximately constant, even if the position of the centres shifts. The ratio of the widths (figure 7.20 C) of crystalline peaks fitted with $\mu c - UAmorf - amorph$ method, using the $\mu c - UAmorf - amorph$

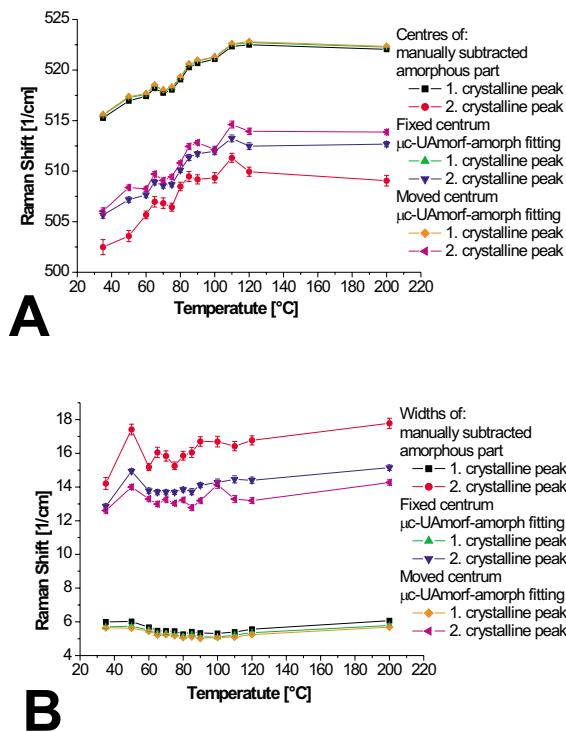


Figure 7.19: The position of centres of the Manabu temperature series (A) and the widths (B) of crystalline peaks fitted with μ c – UAmorf – amorph method, the μ c – UAmorf – amorph method, but moved and then fixed the centre of the UAmorf function so that the difference of maxima of Raman signal and maximum of the amorphous signal stays constant or fitted only crystalline peaks obtained by manual subtracting the amorphous part of the spectra.

method, but with moved and then fixed the centre of UAmorf function or fitted only crystalline peaks obtained by manually subtracting the amorphous part of the spectra stays approximately constant, but the ratio is different for all used methods.

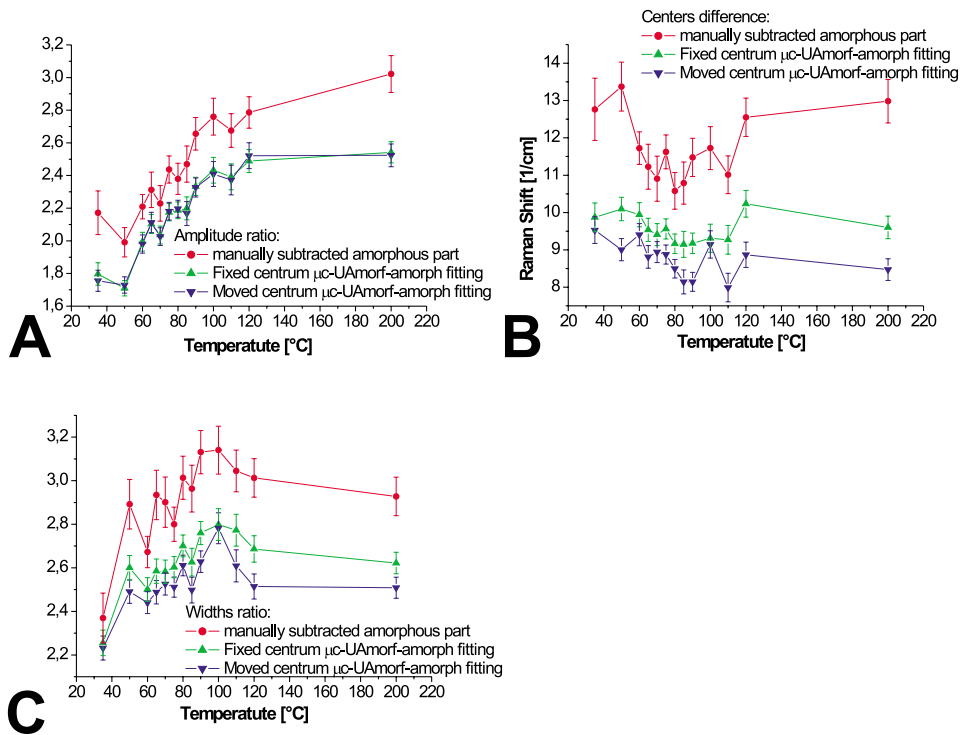


Figure 7.20: The ratio of the amplitudes (A), the difference of the centres (B) and the ratio of the widths (C) of crystalline peaks fitted with μ c-UAmorf-amorph method, using the μ c-UAmorf-amorph method, but with moved and than fixed the centre of UAmorf function or fitted only crystalline peaks obtained by manually subtracting the amorphous part of the spectra of the MTS are behaving similarly for all used methods.

7.8 RF STM Temperature Series (RFTS)

This is also the temperature series, but this series was prepared in our laboratory. It is composed of one amorphous sample (Stm242) and eight microcrystalline samples. The measurement conditions of the series are presented in the table 7.9.

Table 7.9: Overview of the main measurement conditions of the RF STM temperature series.

Sample	Laser power [%]	Laser spot radius [μm]	Exposure time [s]
Stm242	10	1	250
Stm241	10	1	250
Stm246	10	1	250
Stm238	10	1	250
Stm237	10	1	250
Stm236	10	1	250
Stm235	10	1	250
Stm233	10	1	250
Stm232	10	1	250

The raw Raman spectra with the constant background subtracted are shown in the figure 7.21 A. We have manually subtracted the amorphous spectrum of sample Stm242 as described previously (figure 7.21 B). The spectra have been normalized (figure 7.21 C). The shift of the maximum of Raman signal caused by the deposition temperature was found. This shift is similar to the shift in the Manabu Temperature series.

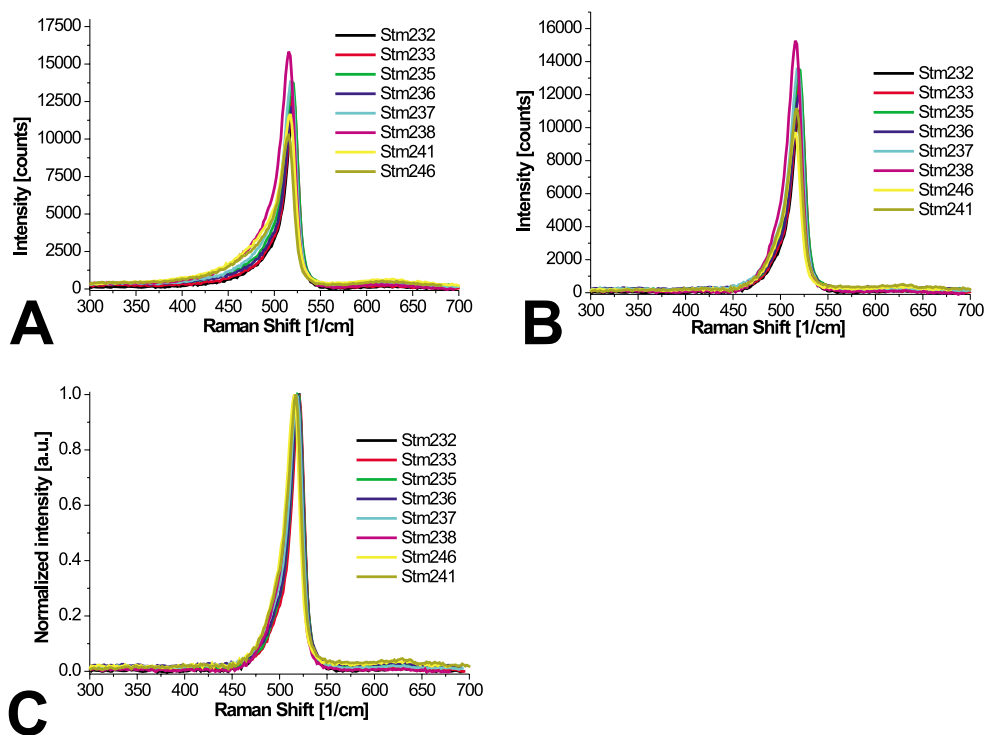


Figure 7.21: In the figure A the raw microcrystalline spectra of the samples of the STM RFTS are presented. Afterwards the amorphous spectrum Stm242 multiplied with an amplitude (adjusted to fit the data) was subtracted, the fully microcrystalline phase of the spectra remained (B). Then the amplitude of the signal was normalized (C).

For comparing the shape of the pure microcrystalline spectra we have shifted the spectra so that they have the same maximum. The detailed look in the spectra before the shift (A) and after the shift (B) is presented in the figure 7.22. According to the figure 7.22 the spectra have similar shape but not exactly the same, as we have observed in the previous series.

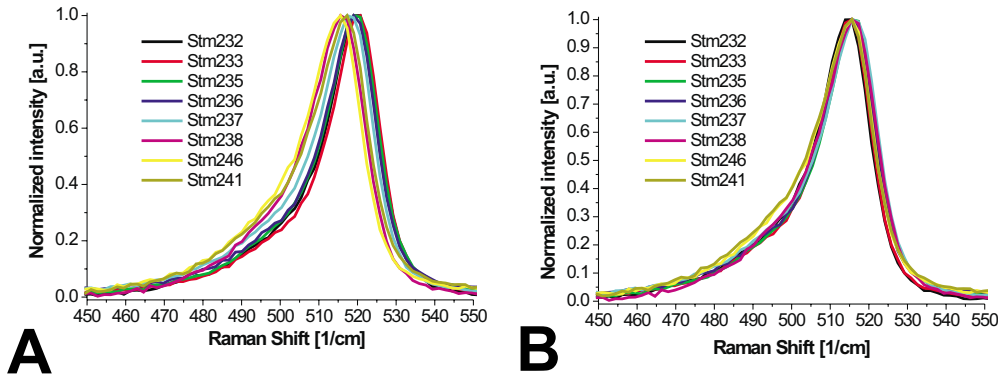


Figure 7.22: The detailed part of the spectra of the RFTS before (A) and after (B) the shift of the Raman spectra to the same maximum of the Raman signal.

We have fitted the fully microcrystalline phase spectra (not shifted to the common maximum of the Raman signal) and also the whole microcrystalline spectra (using the $\mu c - UAmorf - amorph$ method). As the maximum of the Raman signal was not the same for the spectra of this series, we have also fitted the whole microcrystalline spectra using the $\mu c - UAmorf - amorph$ method, but we have moved and then fixed the centre of the UAmorf function such the difference of the maximum of Raman signal and the maximum of the amorphous component stays constant. Simpler to explain, we have shifted the amorphous signal as the maximum of the crystalline signal was shifted. The results of these fits are shown in the figure 7.23. The position and width of the second crystalline peak is slightly different using different methods.

The fact, that the microcrystalline spectra of the STM RF temperatures series do not have exactly the same shape is evident from the fitting results of the parameters, which can better describe the relation between the two Gaussians. The ratio of the amplitudes (figure 7.24 A) as a function of the temperature increases approximately linearly. The difference of the centres (figure 7.24 B) stays approximately constant, even if the position of the centres shifts. The ratio of the widths (figure 7.24 C) of crystalline peaks fitted with $\mu c - UAmorf - amorph$ method, using the $\mu c - UAmorf - amorph$ method, but with moved and then fixed the centre of UAmorf function or

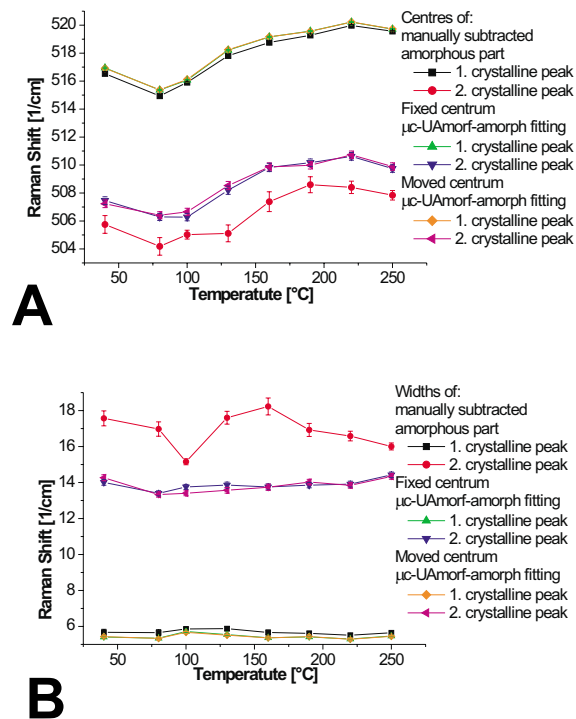


Figure 7.23: The position of centres of the RF STM temperature series (A) and the widths (B) of crystalline peaks fitted with $\mu c - UAmorf - amorph$ method, the $\mu c - UAmorf - amorph$ method, but moved and then fixed the centre of the UAmorf function such the difference of maximum of Raman signal and maximum of the amorphous signal stays constant or fitted only crystalline peaks obtained by manual subtracting the amorphous part of the spectra.

fitted only crystalline peaks obtained by manually subtracting the amorphous part of the spectra stays approximately constant, but the ratio is different for all used methods.

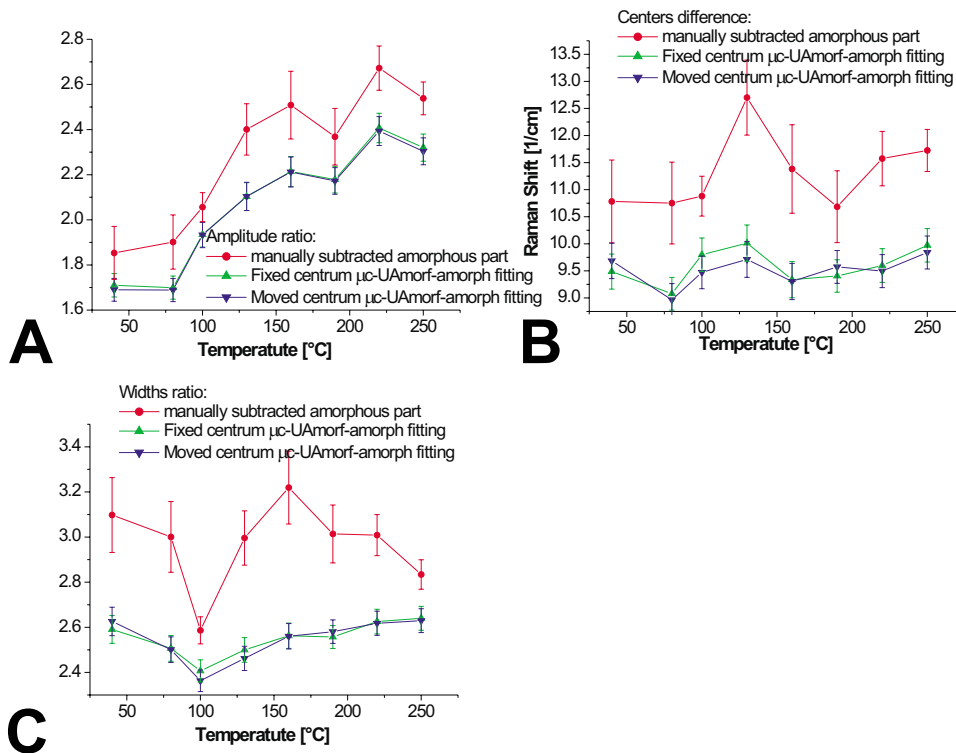


Figure 7.24: The ratio of the amplitudes (A) the difference of the centres (B) and the ratio of the widths (C) of crystalline peaks fitted with μ -UAmorf-amorph method, using the μ -UAmorf-amorph method, but with moved and than fixed centre of the UAmorf function or fitted only crystalline peaks obtained by manually subtracting the amorphous part of the spectra of the RFTS are similarly behaving for all used methods.

This result is very similar to the result of the Manabu temperature series.

Chapter 8

Discussion

8.1 Background

The subtraction of the Raman spectra background can be difficult, even making the detailed study of the spectra impossible. The reason is that the background can be spectrally dependent with a complicated shape and by subtracting it a systematic error can be introduced. Fortunately, we found out that when measuring with the commercial Raman experimental setup (System RM 1000) in the MicroRaman laboratory of the Academy of Sciences the background seems to be only constant, in contrast to the experimental setup in the Raman spectroscopy laboratory of the Charles University, where the background was at least linear but mainly parabolic, or even more complicated.

In this thesis we have therefore used only the spectra measured by micro-Raman setup with constant background subtracted, which made it possible to avoid the discussion about the correct background subtraction and resulting systematic error.

8.2 Amorphous Samples

As was shown in figure 7.1 the normalized spectra of the amorphous samples made by PECVD have very similar shape. However, the spectra are not exactly the same, because of the small shift of the maximum of the TO phonon. All spectra have the maximum of the TO signal in the interval from 468 cm^{-1} to 480 cm^{-1} . This shift is probably caused by different deposition conditions. The pressure [8], or the dilution [10] are known to cause similar shifts.

We have fitted the amorphous spectra with four Gaussian curves, one

for LA phonon (centre fixed at 310 cm^{-1}), one for LO phonon (centre fixed at 380 cm^{-1}), and two Gaussians for TO phonon (no parameter fixed), for obtaining information about the TO amorphous phonon. Regarding the two Gaussians for the TO phonon, the fit with only one Gaussian for the TO phonon did not lead to the sufficient agreement with the measured data (figure 7.2).

8.3 Subtracting the Amorphous Part of the Microcrystalline Spectrum

Assuming that the amorphous parts of the microcrystalline spectra are similar, because of very good similarity in the fully amorphous spectra, the amorphous part can be subtracted after multiplying with an amplitude to fit the microcrystalline spectra. For the series of the samples where only one of the deposition parameters varies, the best spectrum to subtract is the amorphous spectrum of the series. If the series does not contain an amorphous spectrum the best measured spectrum, with the smallest error of each point should be subtracted. In the RF STM temperature series and the Manabu temperature series we have shown, that the deposition temperature can slightly shift the TO crystalline phonon, which can imply that the amorphous part of the spectrum could be shifted as well. However, the results of the fitting of these two series show, that the difference between the resulting fitting parameters of the first approach, where the centre of the amorphous TO phonon is fixed to the same wavenumber as in the amorphous spectrum, or the second approach, where the the centre of the amorphous TO phonon is moved as the crystalline peaks moves, is very small. This result can be caused by the fact that the maximum shift in both series was less than 10 cm^{-1} . This shift is approximately the same as the interval where the maxima of the amorphous TO phonon of our pure amorphous samples was found.

However, the shift does not have to be the same for the TO amorphous and TO crystalline phonon. In [26] was shown, that the location of the TA and TO amorphous phonons in the temperature series can behave differently.

8.4 Complications of the Micro-Raman Measurements

Some of our microcrystalline thin film samples are composed of fully amorphous parts and small crystalline grains, which can be few and far between. Measuring such samples it was possible to choose the place for the micro-Raman measurement which were fully amorphous and have also fully amorphous Raman signal, even if the whole sample was not fully amorphous. As the laser spot on the sample gets smaller, the probability of the incorrect information about the crystallinity of the sample increases.

It is also possible to influence the measured spectra by increasing the laser power density. The measurement of the MicroRaman laboratory allows us to increase the laser power density in two different ways. The first possibility is to increase the focus of the laser, so that the laser spot changes its radius from ten to one microns. The second possibility is to increase the intensity of the laser. The maximal laser power is approximately 10 mW. Both of these methods have been studied. When the laser power density increases, the signal from the TO crystalline phonon shifts to smaller wavenumbers. The shape of the Raman spectra is also influenced. The intensity of the LA phonon is greater and the shape of the LA phonon is sharper than at the low laser power density conditions. We have observed that at the greatest laser power densities the whole Raman microcrystalline spectra including the signal from the hydrogen-associated phonon, shifts to lower wavenumbers by approximately 20 cm^{-1} .

At very high laser power densities, it is even possible to crystallize the sample. As the laser power density on the amorphous sample increases, the sample is locally heated and the obtained Raman signal is more and more crystalline-like. After such a laser power density experiment, if the sample is measured on the same place again, but at the low laser power density conditions, the Raman signal is again fully amorphous-like.

Measuring the Raman signal from larger areas of the sample can avoid obtaining misleading data from small inhomogenous parts of the sample. As the area of the spot is greater the laser power density gets lower. Higher laser power densities can cause the heating of the sample, what can influence the measured spectra, even the crystallization of the sample can be caused.

8.5 Different Fitting Methods

There are at least three methods to fit the microcrystalline spectrum. The difference between them is in the way how to subtract the amorphous part of

the spectrum. In the first method the amorphous spectrum multiplied with an amplitude is manually subtracted and the fully microcrystalline phase of the spectra remains. This fully microcrystalline phase signal is then fitted with two Gaussians. The last two methods fit the amorphous part of the spectrum as a function. The difference between them is in the fixed position of the TO amorphous phonon. If the series where the centre of the TO crystalline signal shifts was fitted, the method using the TO amorphous phonon as a function with centred position to the same wavenumber can be used, or the centre of the TO amorphous phonon function can be shifted as the crystalline TO phonon shifts, but there is only a small difference in the fitting parameters using these two methods.

Differences between the fitted parameters using the manually subtracted amorphous part method or methods, where the amorphous part is fitted as an *UAmorf*-function are shown in our results. It can be caused due to the manual background subtracting.

The comparison of the fitting result for different series and different fitting methods is shown in table 8.1. The errors of centres differences are always greater for manually subtracted background. For the widths ratios are the errors of fits of the manually subtracted amorphous part greater or similar to the errors of other fitting methods. The centres difference for all fitted series are similar. There are only small differences between the fitting results of the $\mu c - UAmorf - amorph$ -(b) method, and the $\mu c - UAmorf - amorph$ method, but with moved and then fixed the centre of *UAmorf* function for the RFTS and MTS. The difference can be caused by the maximum shift of the crystalline peak, where for the RFTS and MTS the shift of the Raman signal of the TO crystalline phonon was approximately 10 cm^{-1} . Probably, if the shift is not too big, the function *UAmorf* does not have to be moved.

That means that there is only one fitting parameter for the whole amorphous part of the sample – the amplitude. The ratio of the widths is also similar for all used methods.

When fitting the microcrystalline spectrum with $\mu c - UAmorf - amorph$ method, the amorphous TO phonon is well described only with one fitting parameter and the TO crystalline phonon is fitted with two gaussian curves, what is six parameters for the crystalline TO phonon. We could decrease the number of fitting parameters from nine (if the microcrystalline spectrum is fitted with three gaussians), to seven. As the difference of the crystalline peaks and the ratio of the widths of the crystalline peak behaves constant, the number of the fitting parameters can be reduced to five.

Table 8.1: Overview of the fitting results for series MTS, RFTS, MDS, Stm254 and Stm282. Obtained differences of the centres with errors and ratios of the widths with errors (standard deviation) of crystalline peaks fitted with $\mu c - UAmorf - amorph-(b)$ method, using the $\mu c - UAmorf - amorph$ method, but with moved and than fixed centre of $UAmorf$ function-(c) or fitted only crystalline peaks obtained by manual subtracting the amorphous part of the spectra-(a) for all series.

series	fitting method	centres difference [1/cm]	error centres difference [1/cm]	width ratio	error width ratio	amplitudes ratio behaviour
RFTS	a	11.3	0.7	3.0	0.2	increase
RFTS	b	9.6	0.3	2.5	0.1	
RFTS	c	9.5	0.3	2.5	0.1	
MTS	a	11.7	0.9	2.9	0.2	increase
MTS	b	9.6	0.4	2.6	0.1	
MTS	c	8.8	0.5	2.5	0.1	
MDS	a	14.6	2.6	2.9	0.3	constant
MDS	b	10.1	0.8	2.3	0.3	
Stm254	a	11.1	3.0	2.8	0.3	constant
Stm254	b	7.7	0.9	2.3	0.3	
Stm282	a	8.7	1.2	3.0	0.2	constant
Stm282	b	9.1	1.1	2.9	0.3	

8.6 Crystallinity Evaluation

Using the previously described fitting methods the TO amorphous and TO crystalline signals can be obtained. The areas from the TO phonons (S_C , S_A) gained by fitting as we suggest can be used for evaluating the crystallinity of the microcrystalline silicon thin films samples from the equation 2.8.

$$X_C = \frac{S_C}{S_C + yS_A}$$

The discussion about this crystallinity evaluation method is not finished yet. An independent method for evaluating crystallinity is needed for comparison with our results. The evaluation of the crystallinity from the XRD measurements can be such a method, but its sensitivity is limited and therefore it requires bigger and thicker samples than available in our laboratory.

Another possible independent method is the AFM microscopy. The AFM microscope measuring in the conductive mode, where the difference between the amorphous and microcrystalline conductivity provides a contrast allow-

ing easy distinction of the phases, can be used for the crystallinity evaluation [16], too. In our laboratory such a microscope is available, but the measurements are complicated, because the microscope is placed in the ultra high vacuum (UHV). It is also difficult to gain a good contrast of the crystalline grains to the amorphous phase for highly crystalline samples. Moreover, the AFM measures surface crystallinity, i.e., the fraction of surface occupied by crystallites, while the Raman scattering probes the sample to a certain depth characterized by the absorption depth of the incident laser beam. At the wavelength 514.7 nm used for our measurements the absorption depth is about 200 nm and the evolution of the shape of the grains with the growing thickness has to be taken into account [27]

8.7 Future Plans

One of our future plans is therefore to measure the series of the samples using our UHV-AFM microscope and compare the values of the crystallinity from the pictures to the values from fitting method as we suggested.

It is necessary to improve our Raman spectra database of more series of the samples, where the correlations between fitting parameters of the microcrystalline thin films spectra could be studied.

It is also important to study fully amorphous spectra because of more information about the amorphous phonons, their shapes and contribution of the spectra. As the shape of the amorphous spectra can change due to deposition parameters, it is important to know how big are the differences, because by the subtracting the amorphous part of the microcrystalline spectra this is the place where the biggest systematic error can be imputed.

It is essential to study the Raman spectra of the samples prepared at different deposition conditions. The deposition parameters can influence not only the crystallinity, but also the shape of the spectra.

Fact that the TO amorphous phonon and also the TO crystalline phonon are both well described with two Gaussians is also interesting and therefore it is worth future studying.

Our fitting program DOORS is functional, but not fully finished yet. In the future we want to upgrade it, make it more user friendly and also more secure and stable. Also it is necessary to make the imputing of the optional new functions simpler and more comprehensive.

Chapter 9

Conclusion

The simplest way to determine the crystalline volume fraction of the microcrystalline silicon sample is its evaluation from the Raman spectra. The computing of the crystallinity from the Raman spectra is not unambiguous and different laboratories use different methods which do not give the same values of this important parameter.

In this work we have studied Raman spectra of series of the samples where one of the deposition parameter was changing, and created the database of Raman spectra.

We have created the program for the decomposition of the ordinary Raman spectra (DOORS) built on the Marquardt-Levenberg fitting algorithm. This program was designed for fitting a large quantity of Raman spectra.

We have introduced a new method for the Raman spectra decomposition into the amorphous and microcrystalline components. We have verified that the amorphous spectra for most amorphous samples have a very similar shape which can be well approximated by four Gaussian bands. The amorphous-like spectrum was also used to describe the amorphous component of the spectra of the mixed phase samples. By subtracting the amorphous component we have obtained the fully microcrystalline component of the spectra with a shape which can be described by two Gaussian bands. This approach provides a better fit of the mixed phase spectra with less parameters than the standardly used three-Gaussian fitting procedures. The areas of the components can be then used for obtaining crystallinity, however, this goal will require future study as it requires an independent method for crystallinity evaluation.

The samples where the nucleation density was influenced by the plasma discharge inhomogeneity and the grains dimension stayed approximately the same dimension were introduced.

The author's contribution was to measure all Raman spectra, create the fitting program DOORS and study the measured spectra using this program.

Bibliography

- [1] M. Vaneček, *Českovenský časopis pro fyziku* **2**, 92 (2002).
- [2] M. Green, K. Emery, D. King, S. Igari, and W. Warta, *Progress in Photovoltaics: Res. and Appl.* **9**, 49 (2001).
- [3] A. Shah, R. Platz, and H. Keppner, *Sol. Energy Mater. Sol. Cells* **38**, 501 (1995).
- [4] T. Mates, A. Fejfar, I. Drbohlav, B. Rezek, P. Fojtík, K. Lutherová, J. Kočka, C. Koch, M. Schubert, M. Ito, K. Ro, and H. Uyama, *J. Non-crystal. Solids* **767**, 299 (2002).
- [5] H. Fujiwara, M. Kondo, and A. Matsuda, *Phys. Rev. B.* **63**, 115306 (2001).
- [6] A. T. Hubbard and J. E. Pemberton, *The Handbook of Surface Imaging and Visualization* (CRC Press, USA, 1995).
- [7] W. H. Weber and R. Merlin, *Raman Scattering in Materials Science* (Springer, London, 2000).
- [8] T. Ishidate, K. Inoue, K. Tsuji, and S. Minomura, *Sol. Stat. Com.* **42**, 197 (1982).
- [9] R. A. Street, *Hydrogenated amorphous silicon* (Cambridge University Press, Cambridge, 1991).
- [10] K. Morigaki, *Physics of Amorphous Semiconductors* (Imperial College Press, London, 1999).
- [11] X. Xu and S. Wagner, in *Amorphous and Microcrystalline Semiconductor Devices*, edited by J. Kanicki (Artech House, London, 1992), Vol. 2, Chap. Physics and Electronic Properties of Amorphous and Microcrystalline Silicon Alloys, pp. 89–96.

- [12] V. Paillard, P. Puech, R. Sirvin, S. Hamma, and P. R. i Cabarrocas, *J. Appl. Phys.* **90**, 3276 (2001).
- [13] P. D. Persans, in *Amorphous silicon and related materials*, edited by H. Fritzsche (World Scientific Publishing Company, London, 1988), Vol. B, Chap. Raman Scattering as a Probe of Structure in Amorphous Multilayers, pp. 1045–1070.
- [14] P. Lengsfeld, S. Brehme, K. Brendel, C. Genzel, and N. H. Nickel, *Phys. Stat. Sol.* **235**, 170 (2003).
- [15] M. Kondo and A. Matsuda, (*oral communication*).
- [16] M. Ledinský, Master's thesis, Charles University, Prague, 2003.
- [17] R. Tsu, J. Gonzalez-Hernandez, S. Chao, S. Lee, and K. Tanaka, *Appl. Phys. Lett.* **40**, 534 (1982).
- [18] E. Bustarret, M. Hachicha, and M. Brunel, *Appl. Phys. Lett.* **52**, 1675 (1988).
- [19] C. Smit, R. A. C. M. M. van Swaaij, A. M. H. N. Petit, W. M. M. Kessels, and M. C. M. van de Sanden, *Appl. Phys. Lett.* **94**, 2582 (2003).
- [20] T. Itoh, K. Yamamoto, H. Harada, N. Yamana, N. Yoshida, H. Inouchi, S. Nonomura, and S. Nitta, *Solar Energy Materials & Solar Cells* **66**, 239 (2001).
- [21] D. Han, K. Wang, and J. M. Owens, *J. Appl. Phys.* **93**, 3776 (2003).
- [22] C. Droz, E. Vallat-Sauvain, J. Bailat, and L. Feitknecht, *Solar Energy Materials & Solar cells* **81**, 61 (2004).
- [23] D. W. Marquardt, *J. Soc. Indust. Appl. Math.* **11**, 431 (1963).
- [24] M. Ito, C. Koch, V., Švrček, M. B. Schubert, and J. Werner, *Thin Solid Films* **383**, 129 (2001).
- [25] D. Bermejo and M. Cardona, *J. Non-crystal. Solids* **32**, 405 (1979).
- [26] A. Voutsas, M. Hatalis, J. Boyce, and A. Chiang, *J. Appl. Phys.* **78**, 6999 (1995).
- [27] A. Fejfar, T. Mates, O. Čertík, B. R. J. Stuchlík, I. Pelant, and J. Kočka, *J. Non-crystal. Solids* (**in press**), (2004).

Curriculum vitae

Born : Košice, Slovak Republic
Date of birth : 20 December 1980
Nationality: Slovak
E-mail : Ladislav.Fekete@matfyz.cz

Secondary education :

- Mathematical high school Poštová in Košice (1995–1999)

University Studies :

- Charles University, Prague
- Student project : The Temperature Dependence of Photoluminescence Spectra of Nanocrystalline CdS, CdSe
- Student project : Photoluminescence Decay of CdS Nanocrystals
- Participation in a research project at the Institute of Physics, Academy of Sciences of the Czech Republic - Department of Thin Films

Field of specialization :

- Optics and Optoelectronics

Research stays :

- University of Barcelona, summer 2003 (2 months)

Publications :

- Decomposition of Raman Scattering Spectra of Mixed Phase Silicon Thin Films, poster at the 3rd aSiNet workshop on thin Silicon, in Bratislava 2004

IT skills :

- advanced programming knowledge of Delphi
- MS-Windows, Origin, Excel

Language knowledge :

- English, German